Linköping Studies in Science and Technology
Thesis No. 962

Cylinder Pressure and Ionization Current Modeling for Spark Ignited Engines

Ingemar Andersson

Division of Vehicular Systems
Department of Electrical Engineering
Linköpings Universitet, SE–581 83 Linköping, Sweden
http://www.vehicular.isy.liu.se/
Email: ingemar@isy.liu.se

Linköping 2002

Cylinder Pressure and Ionization Current Modeling for Spark Ignited Engines

Department of Electrical Engineering,
Linköpings Universitet,
SE–581 83 Linköping,
Sweden.

ISBN 91-7373-379-2
ISSN 0280-7971
LiU-TEK-LIC-2002:35

Abstract

Engine management systems (EMS) need feedback on combustion performance to optimally control internal combustion engines. Ion sensing is one of the cheapest and most simple methods for monitoring the combustion event in a spark ignited engine, but still the physical processes behind the formation of the ionization current are not fully understood.

The goal here is to investigate models for ionization currents and make a connection to combustion pressure and temperature. A model for the thermal part of an ionization signal is presented that connects the ionization current to cylinder pressure and temperature. One strength of the model is that it after calibration has only two free parameters, burn angle and initial kernel temperature. By fitting the model to a measured ionization signal it is possible to estimate both cylinder pressure and temperature, where the pressure is estimated with good accuracy. The parameterized ionization current model is composed by four parts; a thermal ionization model, a model for formation of nitric oxide, a combustion temperature model and a cylinder pressure function. The pressure function is an empirical function design where the parameters have physical meaning and the function has the main properties of a solution to the cylinder pressure differential equations. The sensitivity of the ionization current model to combustion temperature and content of nitric oxide is investigated to understand the need of sub-model complexity.

Two main results are that the pressure model itself well captures the behavior of the cylinder pressure, and that the parameterized ionization current model can be used with an ionization current as input and work as a virtual cylinder pressure sensor and a combustion analysis tool. This ionization current model not only describes the connection between the ionization current and the combustion process, it also offers new possibilities for EMS to control the internal combustion engine.

Acknowledgements

This work was performed in the supervision of Professor Lars Nielsen at Vehicular Systems, Dept. of Electrical Engineering, Linköping University, Sweden, and in collaboration with Mecel AB, Åmål, Sweden.

I would like to thank Mecel AB and especially Jan Nytomt and Anders Göras for their support and encouragement during the four years of this work. Also, ECSEL (Ecsellence center in Computer science and Systems Engineering in Linköping) deserves acknowledgement for funding the project.

A special thanks is directed to Lars Eriksson for his indefatigable enthusiasm in my research and the numerous inspiring discussions along the way. I would like to thank Professor Lars Nielsen for his supervision and especially for his knowledge about presentation technique and manners, and Erik Frisk, who has given invaluable support in the djungle of LaTeX and a number of UNIX based tools and also the inspiring discussions at Snoddas' about the meaning of life.

I would also like to thank the group of Vehicular Systems for over-all interesting discussions and joyful fellowship. My hosts during the almost four years deserve special thanks; Maj-Lis Vååg, Lars Eriksson and Jan Brugård.

Thank you all for helping me completing this work.

Linköping, May 2002

Ingemar Andersson

Contents

1

Introduction

Internal combustion engines have been a major power source throughout the history of ground vehicles. Since the oil crisis in the 1970's the focus for engine developers have moved to fuel economy and emission reduction. The introduction of electronic ignition and fuel injection systems in the 1980's have given the engineers far more capability of engine control than before. The limitation in engine control development lies in the available information about the controlled process; the combustion.

Fuel economy drives the development of efficiency of the engine. This includes optimal ignition timing and fuel amount for a given operating condition. Emission reduction drives the development of air-fuel ratio control, misfire detection and purge control. Oxygen sensors mounted in the exhaust pipe provide a possibility for closed loop air-fuel ratio control and piezo-electric knock sensors mounted on the engine block, for closed loop knock control, but the need for supervising the combustion process itself increases constantly. Three methods exist for combustion monitoring;

- cylinder pressure sensing
- ionization current sensing
- optical instruments

Optical methods include TV cameras or lasers targeting a transparent part in the cylinder head or wall. This equipment is expensive and only suitable for laboratory work. Cylinder pressure sensors can be mounted in the cylinder head to measure the pressure development during combustion. Most of the commonly

used combustion quality measures are related to the cylinder pressure. The pressure sensor is currently only used in laboratory environments due to cost and lifetime performance, but progress is made to find a sensor suitable to be mounted in future engine management systems (EMS). The only one of the three mentioned sensing methods that is used in production EMS today is the ionization current sensor. For spark ignited engines the spark plug is used as sensor together with some measurement electronics added to the ignition system. It is a relatively cheap method for combustion monitoring and other sensors can be replaced. The use of ion sensing in modern EMS is restricted to knock and misfire detection but engine developers start to see a need for other combustion information, such as air-fuel ratio, torque, combustion stability and location of peak pressure. Research in the area aims to find the requested information in the ionization current and the results are promising. Still, there is much work left to explain and understand the information hidden in the ionization current. This thesis will add a piece to that work.

1.1 Thesis outline

Chapter 2 presents a survey of earlier suggested models for ionization current with the basic thoughts and assumptions and, in the case they were presented, the equations for the model.

One model approach, by Saitzkoff and Reinmann, considers the second peak of the ionization current. It is used as the ionization base in the rest of the modeling work in the thesis. In Chapter 3 the ionization model is investigated in more detail to understand the physical processes. A central part here is the thermal ionization of nitric oxide, NO. NO is a combustion product when carbon based fuel burns in air. The formation of NO is dependent of combustion temperature and the content of NO in the combusted gas is not constant through the combustion. The impact of dynamic or reaction rate controlled NO formation is studied.

The thermal ionization makes the combustion temperature an important parameter. The description of the combustion temperature depends on the chosen combustion model. Chapter 4 investigates three different combustion model approaches in the sense of how they can help to explain the amplitude and position of the ionization current.

Chapter 5 presents a parameterized model for cylinder pressure. The model is not written in the traditional form of a differential equation, but as an explicit function of crank angle and measurable inputs of the combustion process. This chapter was presented as a separate paper at SAE 2001 World Congress, SAE-2001-01-0371.

Finally, Chapter 6 puts the pieces from Chapters 3 - 5 together in one model to connect cylinder pressure and ionization current. The model is composed by the explicit pressure model, a kernel zone combustion model for temperature calculation, a dynamic NO formation model and a model for thermal ionization.

A validation of the model is presented. Certain attention is given to how well the model describes the cylinder pressure based on the ionization current.

1.2 Contributions

The first two contributions are the investigation of the Saitzkoff-Reinmann ionization model properties and how important the models of NO formation and combustion temperature are.

The main contributions lie in Chapters 5 and 6 which describe the development of a parameterized pressure function and the parameterized ionization current model. The parameterized cylinder pressure function presents an empirical solution with physically interpretable parameters to the pressure differential equations.

The parameterized ionization current model describes the ionization current with only two free parameters that handle shift in both ignition timing and air-fuel ratio. One of the parameters is the total burn angle of the combustion, which here is possible to estimate. The model can use a measured ionization current as input and calculate the cylinder pressure with good performance. The modeling work altogether presents a virtual pressure sensor based on measurement of ionization current.

2

Ionization current basics

2.1 Ionization current properties

The combustion in a spark ignited (SI) engine normally starts with a spark discharge in the spark plug. A flame develops and travels from the spark plug location out to the cylinder walls as it consumes the air-fuel mixture. The chemical reactions and the raised temperature in the flame front produce free charges through various ionization processes. The amount of free charges is small but measurable (Reinmann, 1998). By applying a voltage to the spark gap after the spark has vanished, the free charge will form a current, the *ionization current* or *ion current*. The technology for measuring the ionization current is called *ion sense*. Figure 2.1 shows an symbolic ion sense system. The combustion generates free charge, e-. An outer measurement circuit provides the measurement voltage from a capacitor. The current I flows through the circuit and the current equivalent voltage U_ion is measured over the resistor R.

Ion sensing has been a hot topic in recent years concerning measurement techniques and its possible applications (Nielsen and Eriksson, 1998; Asano et al., 1998; Auzins et al., 1995; Balles et al., 1998; Collings et al., 1991; Daniels, 1998; Förster et al., 1999; Hellring et al., 1999; Lee and Pyko, 1995; Shimasaki et al., 1993; Andersson and Eriksson, 2000). More theoretical investigations, concerning physical and chemical modeling, have been performed and reported by Saitzkoff et al. (1997), Reinmann et al. (1998) and Wilstermann (1999).

The ionization current has a characteristic shape. One proposal divides the ion current in three parts, the ignition phase, the flame front phase and the post-flame phase (Eriksson et al., 1996; Nielsen and Eriksson, 1998). Figure

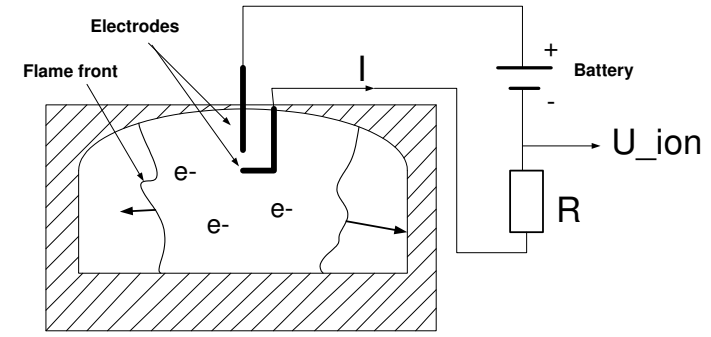

Figure 2.1: *Ion sense system*

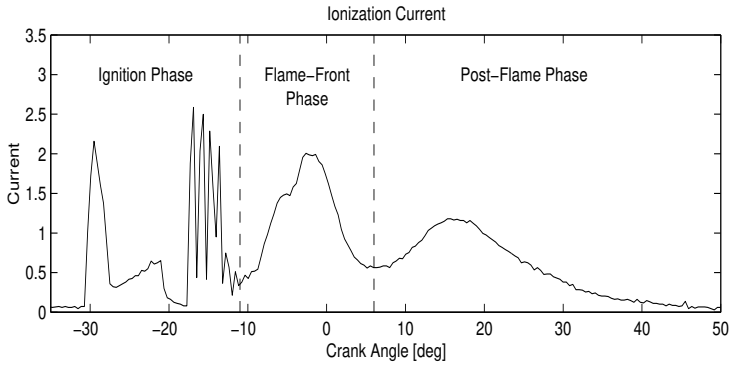

Figure 2.2: *Example of ionization current with its three characteristic phases. (Eriksson (1999))*

2.2 shows a typical ion current trace from a port fuel injected engine with an inductive ignition system. The ignition phase starts with charging the ignition coil and ends with the coil ringing after the spark. The flame-front phase reflects the early flame development in the spark gap and the post-flame phase appears in the burned gases behind the flame front.

The ignition phase is often left out in discussions about ionization currents. This leaves a current shape with typically two peaks. The flame front phase is often referred to as *first peak* or *flame peak*. The post-flame phase has been named *second peak*, *thermal peak* or *post-flame peak*. The flame peak has been modeled as generated from ionization in chemical reactions (Reinmann et al., 1997; Wilstermann, 1999).

Saitzkoff et al. (1996) made the first approach to explain the physics behind the post-flame peak. The approach suggests thermal ionization of nitric oxide

as the source of free charge in the combustion chamber, therefore the name *thermal peak*. The thermal peak also has a strong correlation in position to the cylinder pressure (Eriksson et al., 1996; Nielsen and Eriksson, 1998). This property of the ionization current makes it interesting for use in engine control systems for spark timing control and combustion diagnostics.

2.2 Existing models

The common understanding is that the measured ionization current has its origin in the thermal and chemical ionization processes taking place during the combustion. However, several other processes are active affecting the shape of the current before it is measured by an AD converter. The free electric charge need to move in the electric field caused by the measurement electrodes and cause an electric current to flow in the measurement circuit. Electrons are absorbed at the positive electrode and emitted at the negative.

The modeling work include the decision about which process that is limiting the ionization current at every moment. Earlier research present three different models and they are all based on different assumptions about the limiting process in ionization and the measurement circuit. The following sections explain the three models with their basic assumptions and, when presented earlier, their equations.

2.2.1 Saitzkoff-Reinmann model

A model for the second peak of the ion current was presented by Saitzkoff et al. (1996). Figure 2.3 shows the idea behind the model. A cylinder shaped control volume between the two spark plug electrodes contains free electrons from thermal ionization of NO. The electrical field between the electrodes create a movement of the electrons. The movement of free electrons dominates the current since they are highly mobile compared to positive ions. The dominating process for generating free electrons is the thermal ionization of NO and can be described by Saha's equation (see Saitzkoff et al. (1996) for assumptions)

$$\frac{n_1 n_e}{n_0} = 2\left(\frac{2\pi m_e kT}{h^2}\right)^{\frac{3}{2}} \frac{B_1}{B_0} exp\left[-\frac{E_1}{kT}\right] \tag{2.1}$$

which describes the equilibrium balance of ions and electrons for a first order ionization. When combined with models for electron drift velocity and electric field an expression for ion current is obtained as (Saitzkoff et al., 1996)

$$I = U\frac{\pi r^2}{d}\frac{e^2}{\sigma m_e\sqrt{\frac{8kT}{\pi m_e}}}\sqrt{\phi_s}\sqrt{\frac{2\left(\frac{2\pi m_e kT}{h^2}\right)^{\frac{3}{2}}\frac{B_1}{B_0}\exp\left[-\frac{E_1}{kT}\right]}{n_{tot}}} \tag{2.2}$$

Table 2.1 describes all entries in Equations (2.1) and (2.2).

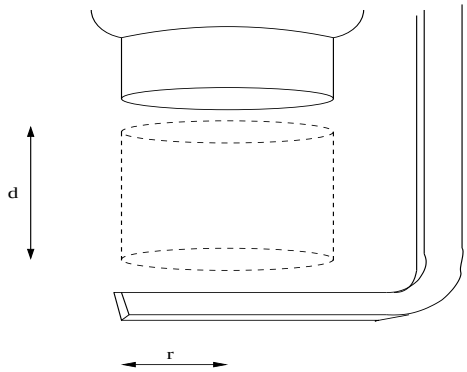

Figure 2.3: *The measurement volume according to Saitzkoff-Reinmann model, between the electrodes in the spark gap*

n_1	Number density of ions	T	Temperature of gas
n_e	Number density of free electrons	ϕ_s	ratio of NO i gas mixture
		m_e	electron mass
n_0	Number density of neutral particles	B_i	internal partition function
		E_1	Ionization energy for 1st order ionization
U	Measurement voltage		
r	Radius of measurement cylinder	n_{tot}	total particle number density
d	Length of measurement cylinder	k	Boltzmann's constant
		h	Planck's constant
σ	collision cross section	e	unit charge constant

Table 2.1: *Parameter set in Saitzkoff-Reinmann model*

The model sees a free space charge that is affected by the electrical field generated by the measurement probe, the spark plug. The movement of the charge does not change the field inside the combustion chamber significantly since the re-distributed charge is at such a low magnitude. The movement is however measurable in the outer circuit. The main limit for the current is the access of free electrons. This is the main difference compared to other models.

Wilstermann (1999) presented a similar model. The model uses more detailed calculations on electric field and has added chemical reactions in the flame front as a source for free charge.

2.2.2 Calcote model

The model presented by Calcote (1963) considers the electrode physics when electrons enter or leave the electrodes of the measuring circuit. The model of this process has been used by Wilstermann (1999) to explain the occurrence of ionization current in a spark plug measurement circuit.

The spark plug is modeled as a Langmuir probe. The central electrode has some electrical potential U_s relative the chamber walls and grounded parts of the spark plug. The combustion chamber contains a distribution of partly ionized gases, where there are positive and negative ions and free electrons. At low center electrode potential the movement of the particles is dominated by temperature. A limit for the measurement voltage when the particle movement becomes dominated by the electric field was not presented.

If U_s is negative enough no electrons will reach the center electrode surface, since all electrons will be repelled by the electrical field. Positive ions will be attracted to the electrode and produce some current. When U_s increases towards positive the fastest electrons will start to overcome the electrical field and reach the surface of the center electrode. At some point when U_s is still negative, the current contribution from electrons and positive ions are equal and the net current is zero. This point is called the Floating potential. At $U_s = 0$ the electron current dominates over the positive ion current due to the higher mobility and higher temperature.

The electrical field around the center electrode will cause a redistribution of charge in the combustion chamber. Charge with opposite sign to U_s will gather around the electrode and eliminate the field in the rest of the combustion chamber. For $U_s > 0$, the electron concentration n_e around the electrode will increase as U_s increases. The current is then limited by the surface process of the electrode. The surface process at the electrodes can be described as

$$I_e = n_e e A_s \sqrt{\frac{kT_e}{2\pi m_e}} \left[1 + \frac{3ld}{16\lambda_e B_e} ln\left(\frac{X_e + B_e}{X_e - B_e}\right)\right]^{-1}$$

$$I_i = n_i e A_s \sqrt{\frac{kT_i}{2\pi m_i}} \left[1 + \frac{3ld}{16\lambda_i B_i} ln\left(\frac{X_i + B_i}{X_i - B_i}\right)\right]^{-1}$$

where all entries are listed in Table 2.2. The first equation is valid for electrons

n_e	electron concentration
m_e	electron mass
T_e	Electron temperature
λ_e	electron mean free path
e	unit charge
l	probe length
d	probe diameter
A_s	probe surface area

X_e	$= l + 2\lambda_e$
B_e	$= \sqrt{X_e^2 - (d + 2\lambda_e)^2}$
n_i	ion concentration
m_i	ion mass
T_i	ion temperature
λ_i	ion mean free path
X_i	$= l + 2\lambda_i$
B_i	$= \sqrt{X_i^2 - (d + 2\lambda_i)^2}$

Table 2.2: *Parameter set in Calcote model*

at a positive electrode and the second is valid for positive ions at a negative electrode.

Typically, ion current measurement systems of today use a positive center electrode potential. The electron current at the positive electrode dominates the total current due to the lower mass and higher temperature of the electrons compared to the ions. As the measurement voltage U_s increases, the electron concentration around the electrode n_e increases and therefore the current. The assumption here is that the access of free electrons in the combustion chamber is sufficient for the needed redistribution. No equation for the relation between n_e and U_s was given.

2.2.3 Yoshiyama-Tomita model

Yoshiyama et al. (2000) presented a theory based on flame front ionization. Experiments were made in a combustion bomb as in Figure 2.4. The combustion bomb has a spark gap between two electrodes which are isolated except for the top where the spark is fired. The bomb wall can be electrically isolated or connected to one of the electrodes. An air-fuel mixture was ignited and the ionization current was measured between the electrodes for different electrical configurations of the chamber wall. A camera was monitoring the flame propagation and the pictures were synchronized with the measured current. The resulting current shows the two characteristic peaks, in some cases. The first ion peak appears when the flame front is close to the spark gap in all tests. The second peak appears only for the case when the wall is connected to the negative electrode and when the flame front reaches the wall. From the experiments two conclusions were drawn:

- The ionization current shape is dependent of flame position and electrode polarity.
- Ions and electrons are generated in the flame front by chemical reactions and thermal ionization is negligible.

The presented theory explains the results from the experiments made. However, the conditions in the experiments, start pressure of 4 bar and start tem-

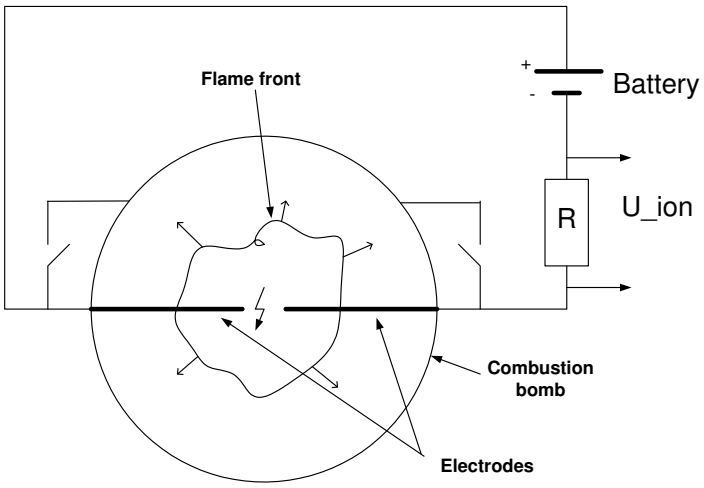

Figure 2.4: *Experimental setup used by Yoshiyama and Tomita*

perature of 290 K, may lead to that the proposed thermal ionization will not take place due to low temperature. Formation of NO will also be much less than for the experiments done by Saitzkoff et al. (1996).

2.2.4 Other observations

Experiments on engines using different types of spark plugs show a strong geometry dependency in the measured ionization current. Following conclusions have been drawn:

1. Larger center electrode increases amplitude of thermal peak. This fact supports all three theories.

2. Larger ground electrode increases flame peak amplitude. This is supported by both Calcote and Yoshiyama-Tomita models. The Saitzkoff-Reinmann model does not include the flame front phase.

3. The shape of flame peak depends on the shape of ground electrode. This is also supported by both Calcote and Yoshiyama-Tomita models.

4. The shape of the thermal peak depends on the supply of electrons from easily ionized species as NO and alkali metals. This fact is immediately explained by the Saitzkoff-Reinmann model, but the other two models are also valid.

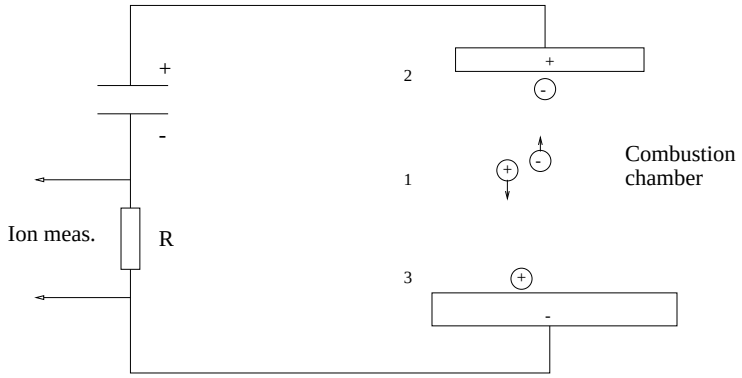

Figure 2.5: *View of three processes occurring in ionization measurement.*

2.3 Summary and model discussion

The three models have different views of the ion current generating process in the cylinder and measuring circuit. Figure 2.5 shows the three main processes considered in the models.

The Reinmann model assumes that a current is detectable in the measuring circuit if a charge is moving in the electric field inside the cylinder (process 1). The charge need not to be in contact with the electrodes.

The Calcote model considers the gas-electrode transition and charge transport process to be most important. This means that the charge needs to reach the electrode to make a current detectable (processes 2 and 3). Mobility becomes an important property. The Calcote model also states that the current at the two electrodes need not to be equal. The most mobile charge, the electron, will dominate the ion current.

The Yoshiyama and Tomita model states that the current at the two electrodes need to be equal since the current appears to be limited by the slower positive ions in the flame front (processes 2 and 3).

These three processes are different but not necessarily excluding each other. They may co-exist in some sense. However, the three models have different interpretation of the ionization current in the sense of combustion parameters. As an example is the second peak of the ionization current strongly related to the cylinder pressure peak in the Saitzkoff-Reinmann model but for the Yoshiyama-Tomita model it implies that the flame front has its maximum contact area to the chamber walls. This is not the same thing. To explore this idea further it is necessary to know how the measurement circuit works, but this investigation is left for future work.

3

NO formation and thermal ionization

This section presents an analysis of the ionization current model suggested by Saitzkoff and Reinmann in more detail. The base is thermal ionization of nitric oxide, NO. The model is built up by two processes, NO formation and thermal ionization, with combustion temperature and air-fuel ratio as inputs. The two processes are summarized here and finally the temperature sensitivity is discussed.

The composition of the burned gases is changed during the progress of a combustion. The formation of major exhaust gas components have been described with chemical reactions, balanced by temperature dependent equilibrium constants by Lavoie et al. (1970) and Heywood (1988). Most reactions, except for NO formation, are described as fast compared to the time-scale of a combustion and concentrations are close to equilibrium. The formation of NO is slower and is better described as reaction rate limited rather than in equilibrium. Two questions are addressed here:

1. Is NO the most probable main contributor of free charge from thermal ionization?
2. What impact does combustion temperature and NO content have on ionization current amplitude?

3.1 NO formation theory

Heywood (1988) gave a description of the process behind NO formation, based on the Zeldowich mechanism (Zeldovich et al., 1947). This is a summary of

the processes described by Heywood and this model is referred to as the *dynamic NO formation* or *reaction rate controlled NO formation* in this thesis. The description by Heywood (1988) does not cover formation of all species in the reactions. Concentrations of different species, needed as inputs, were calculated by the Matlab program package *CHEPP* (Eriksson, 2000). To validate the implementation of the dynamic NO formation model, the calculation of equilibrium concentration of NO is compared between the Heywood model and the CHEPP tool. Also Figure 11.7 in (Heywood, 1988) was produced as a reciept that the implementation was equal to the one by Heywood.

The extended Zeldovich mechanism (Zeldovich et al., 1947; Lavoie et al., 1970) lists the dominating reactions for forming NO:

$$O + N_2 \rightleftharpoons NO + N$$
$$N + O_2 \rightleftharpoons NO + O$$
$$N + OH \rightleftharpoons NO + H$$

Two assumptions are made:

1. the content of N is small and changes slowly compared to the content of NO
2. concentrations of O, O_2, OH, H and N_2 can be approximated by their equilibrium concentrations

With these assumptions the following expression for NO formation is derived:

$$\frac{d\,[NO]}{dt} = \frac{2R_1(1 - ([NO]/[NO]_e)^2)}{1 + ([NO]/[NO]_e)R_1/(R_2 + R_3)} \tag{3.1}$$

where

$$R_1 = k_1^+[O]_e[N_2]_e = k_1^-[NO]_e[N]_e$$
$$R_2 = k_2^+[N]_e[O_2]_e = k_2^-[NO]_e[O]_e$$
$$R_3 = k_3^+[N]_e[OH]_e = k_3^-[NO]_e[H]_e$$

The concentration [ ] is in the unit $[mol/cm^3]$ and the reaction rate constants are listed in Table 3.1 (Heywood, 1988). The concentration $[NO]$ is defined as

$$[NO] = \frac{N_{NO}}{V} \tag{3.2}$$

where N_{NO} is the quantity of NO in [mol] distributed in the volume V. For a constant volume V Equation (3.1) can equivalently be written as

$$\frac{1}{V}\frac{dN_{NO}}{dt} = \frac{2R_1(1 - ([NO]/[NO]_e)^2)}{1 + ([NO]/[NO]_e)R_1/(R_2 + R_3)} \tag{3.3}$$

	Rate constant $[\frac{cm^3}{mol \times s}]$
k_1^+	$7.6 \times 10^{13} exp[-38000/T]$
k_1^-	1.6×10^{13}
k_2^+	$6.4 \times 10^{9} exp[-3150/T]$
k_2^-	$1.5 \times 10^{9} exp[-19500/T]$
k_3^+	4.1×10^{13}
k_3^-	$2.0 \times 10^{14} exp[-23650/T]$

Table 3.1: *Reaction rate constants for NO formation.*

The initial concentrations for O_2, OH, H and N_2 can be found using CHEPP, which calculates the species concentration of the above based on air fuel ratio. A calculation of the constants R_1, R_2 and R_3 based on equilibrium conditions for combustion of isooctane at 10 bar pressure and temperature of 2600 K and fuel-air ratios of 0.8 to 1.2, gives Table 3.2. The table is comparable to

Equivalence ratio	R_1	R_1/R_2	$R_1/(R_2+R_3)$
0.8	2.37e-4	2.63e+3	0.863
1.0	1.13e-4	5.39e+3	0.539
1.2	3e-5	1.91e+4	0.268

Table 3.2: *Calculation of R1, R2 and R3, @ 2600 K, 10 bar*

Table 11.2 in (Heywood, 1988), where the same calculations were made. The equilibrium concentrations for O_2, H and N_2 were calculated using CHEPP software. Concentrations for O and NO were calculated by the equations in (Heywood, 1988):

$$[O]_e = \frac{K_{p(O)}[O_2]_e^{1/2}}{(\tilde{R}T)^{1/2}}$$

$$K_{p(O)} = 3.6 \times 10^3 exp\left(\frac{-31090}{T}\right) \text{atm}^{1/2}$$

$$[NO]_e = (K_{NO}[O_2]_e[N_2]_e)^{1/2}$$

$$K_{NO} = 20.3 exp\left(\frac{-21650}{T}\right)$$

The equilibrium concentration calculations for NO was compared between the above expression and the CHEPP calculation. Results are shown in Figure 3.1 and the difference is small. The formation of NO is temperature sensitive. A simulation based on fixed pressure and volume gives a temperature dependency as in Figure 3.2. Fixed pressure and temperature means that the equilibrium

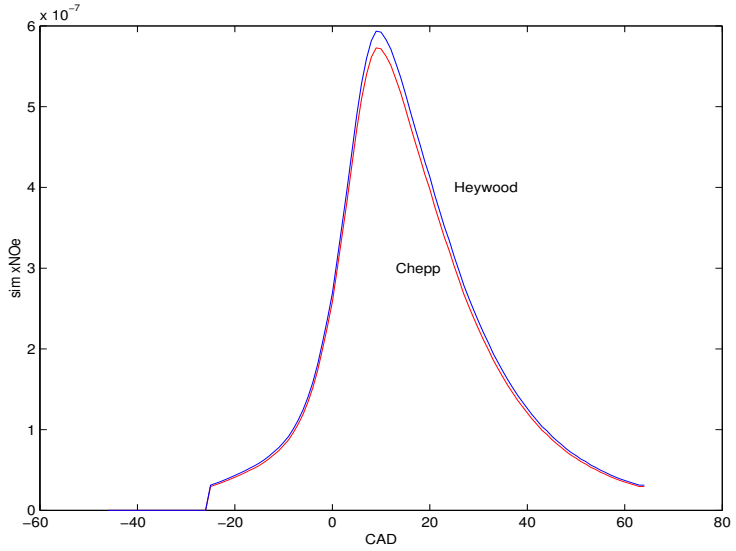

Figure 3.1: *Equilibrium NO concentrations calculated from two different methods.*

concentration of NO is constant and the simulation describes the time for the rate controlled NO formation to reach equilibrium concentration.

NO formation time scale

The time-scale in a combustion is important in this study. An engine speed of 2000 rpm and a burn duration of 70 CAD corresponds to a time-scale of approximately 5 ms. The simulation shows that when the combustion temperature is above 2800 K for the equilibrium concentrations of NO will be reached. A characteristic time at 2800 K is 0.5 ms, the time it takes for the NO concentration to reach 90% of equilibrium. However, typical peak values in combustion temperature occurs around 2600 K (Greenhalgh, 1983) which means that the equilibrium concentration for NO will be reached in the peak values. At temperatures of 2000 K the time delay is 1 second and at lower temperatures the reactions are so slow that the NO formation is considered to be frozen.

NO formation and volume change

The value of the formation rate in Equation (3.1) is close to zero for a frozen mixture. This fact reveals a lack in Equation (3.1). If the gas mixture is frozen but is allowed to expand, the quantity of NO is constant but the concentration will decrease. For the purpose of calculating NO concentration in internal combustion engines an extension of Equation (3.1) is proposed that accounts

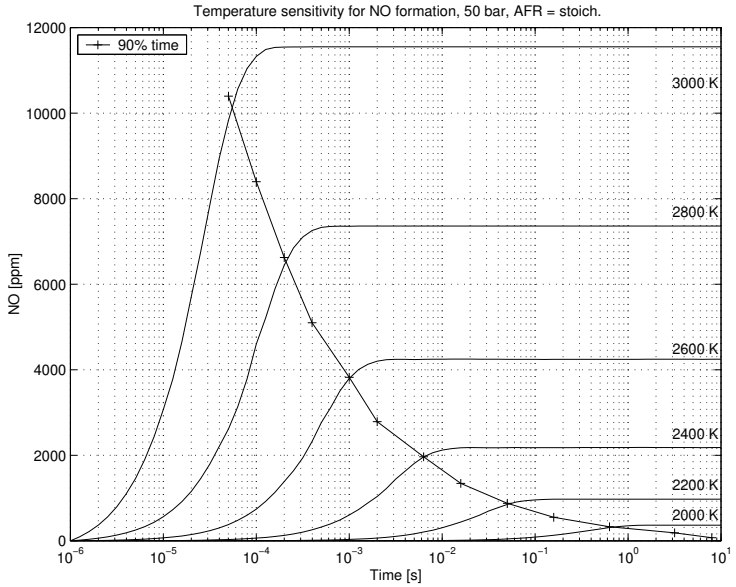

Figure 3.2: *Temperature sensitivity for NO formation. Simulation is based on 50 bar pressure, stoichiometric AFR, a fixed volume and temperature.*

for a change in burned zone volume, V_b. The chain rule gives the derivative of $[NO]$ using Equation (3.2) as:

$$\frac{d[NO]}{dt} = \frac{d}{dt}(\frac{N_{NO}}{V}) = \frac{1}{V}\frac{dN_{NO}}{dt} + \frac{d}{dt}\left(\frac{1}{V}\right)N_{NO} = \tag{3.4}$$

$$= \frac{1}{V}\frac{dN_{NO}}{dt} - \frac{1}{V^2}\frac{dV}{dt}N_{NO} = \tag{3.5}$$

$$= \frac{1}{V}\frac{dN_{NO}}{dt} - [NO]\frac{1}{V}\frac{dV}{dt} \tag{3.6}$$

Here the proposal is to use Equation (3.3) and $V = V_b$ in (3.6) which leads to

$$\frac{d\,[NO]}{dt} = \frac{2R_1(1-([NO]/[NO]_e)^2)}{1+([NO]/[NO]_e)R_1/(R_2+R_3)} - [NO]\frac{1}{V_b}\frac{dV_b}{dt} \tag{3.7}$$

This model gives satisfactory results in simulations of NO concentrations for combustion cycles. An increase of cylinder volume will increase the burned zone volume and the concentration of NO in the burned zone decreases. The volume of the burned zone depends on the chosen combustion model and different choices will be discussed in Chapter 4.

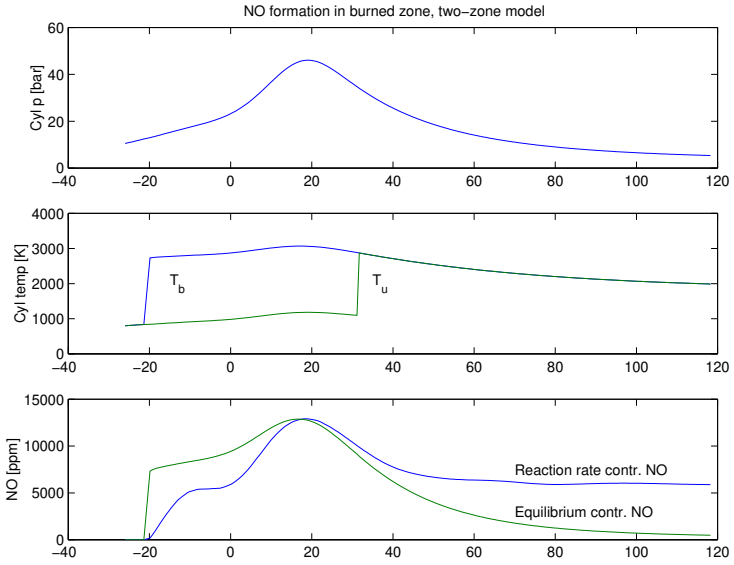

Figure 3.3: *NO formation simulated from engine pressure data*

Validation of model

To verify the implementation of the NO formation model, a figure like 11.7 in (Heywood, 1988) was created. Starting from a pressure trace a temperature trace was calculated using a standard, fully mixed two-zone combustion model.

Figure 3.3 shows the result. Qualitatively it looks the same as Figure 11.7 in (Heywood, 1988). The upper graph is the cylinder pressure and in the middle shows the calculated temperatures, burned T_B and unburned zone T_U. The lower graph shows the NO content in ppm for equilibrium and reaction rate controlled formation. Equilibrium controlled NO formation depends on temperature. Reaction rate controlled NO formation is fast and almost in equilibrium around 20 CAD ATDC where the temperature is high. At 40 CAD the reaction has slowed down significantly and from 70 CAD and forward the mixture seems frozen. At this point the temperature has reached 2100 K and according to Figure 3.2 the reactions still go on but the reaction rate is slow compared to the engine speed. The characteristic time at 2100 K is approximately 0.3 s.

Engine speed dependency

Figure 3.4 shows a simulation of NO formation based on a pressure trace from an engine at relative air fuel ratio of 1.1 and at three different engine speeds; 2000, 4000 and 6000 rpm. The dotted line shows the equilibrium concentration of NO ($[NO]_e$) as a function of crank angle. The three solid lines show the rate

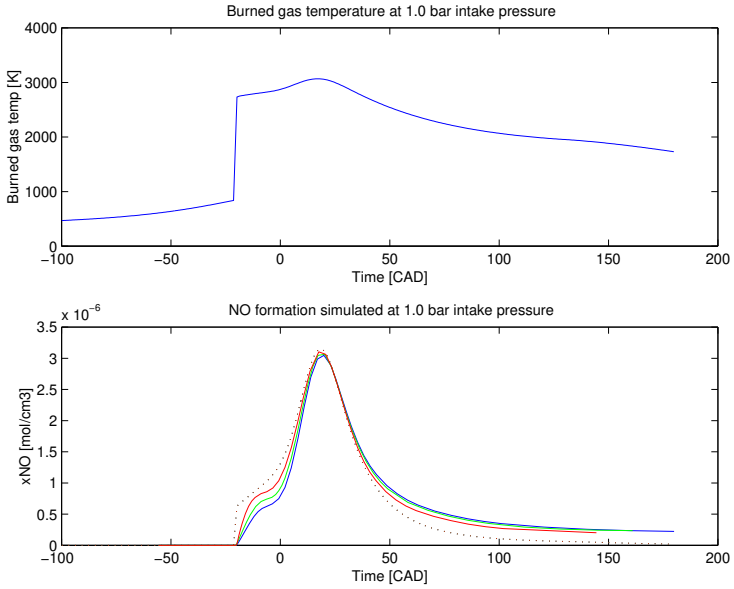

Figure 3.4: *Reaction rate controlled NO formation compared to equilibrium controlled at different engine speeds; 2000, 4000 and 6000 rpm.*

controlled NO concentration ($[NO]$). The slowest combustion happens for the lowest engine speed and $[NO]$ for this case falls closest to $[NO]_e$.

The difference in $[NO]$ for different engine speeds appear when the combustion temperature passes through the region where the characteristic time of NO reactions is in the same order as the time-scale of the combustion. For higher engine speed the temperature will spend less time in this region and $[NO]$ deviates from $[NO]_e$.

3.2 Thermal ionization theory

A detailed description of thermal ionization process was given by Saitzkoff et al. (1996) in appendix A. The balance between generation and regeneration of ions caused by thermal excitation forms the basis for the ionization. The ionization process is assumed to be fast compared to the combustion process and specifically the combustion temperature development. Therefore the electrons and ions are in thermodynamic equilibrium and the balance can be described by the Saha equation

$$\frac{n_i n_e}{n_{i-1}} = 2\left(\frac{2\pi m_e kT}{h^2}\right)^{\frac{3}{2}} \frac{B_i}{B_{i-1}} \exp\left[-\frac{E_i}{kT}\right] \tag{3.8}$$

n is number density for species of ionized state i, i-1 and electrons e. m_e is the electron mass, k is Boltzmann's constant, h Planck's constant, E_i ionization energy for ionized state i, T is the mixture temperature and B is the internal partition function. Saitzkoff et al. (1996) assumed that NO is only ionized to the first level. If the ionization ratio is defined as

$$\eta = \frac{n_e}{n_0 + n_i} \tag{3.9}$$

and assuming only first level ionization

$$n_e = n_i = n_1 \tag{3.10}$$

Combining expressions (3.8), (3.9) and (3.10) gives an expression for ionization ratio η

$$\eta = \sqrt{\frac{n_H}{n_0}}$$
$$n_H = 2\left(\frac{2\pi m_e kT}{h^2}\right)^{\frac{3}{2}} \frac{B_1}{B_0} \exp\left[-\frac{E_i}{kT}\right]$$

where n_0 is the number density of the neutral species.

Using the CHEPP software for equilibrium concentration calculations of burned gas species, some other sources for thermal ionization may be explored. The ionization energy for different species are listed in Table 3.3. The impact

Species	**Ionization energy (eV)**
H	13,6
H_2	15,4
O	13,6
O_2	12,1
OH	13,2
H_2O	12,6
CO	14,0
CO_2	13,8
NO	9,2
N_2	15,6

Table 3.3: *Ionization energies for dominant combustion species, from Wilstermann (1999)*

of ionization energy is seen in Figure 3.5. An increase of 1 eV in ionization energy will decrease the ionization ratio with a factor of 10. One other species with higher ionization energy than NO has to have a correspondingly higher concentration to produce the same amount of ions. Considering Table 3.3 it is seen that from the listed species the closest in ionization energy is O_2 with

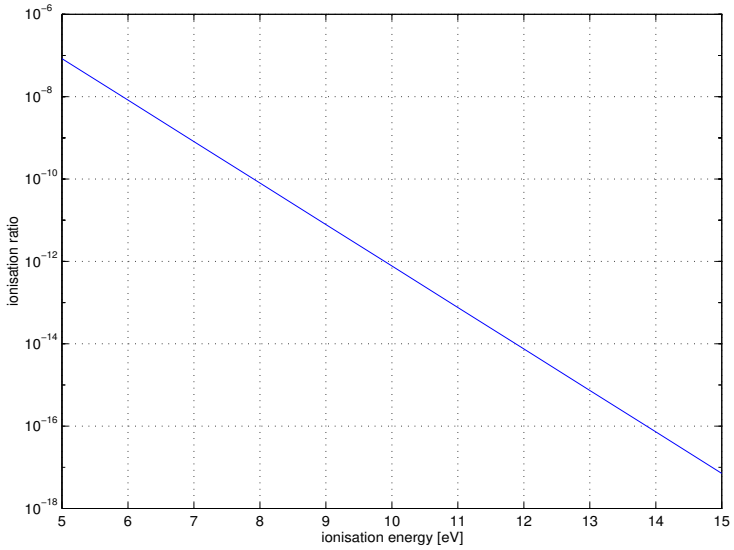

Figure 3.5: *Ionization ratio dependency on ionization energy, @ 2500K, 20 bar.*

12.1 eV. The difference in 3 eV means an ionization degree difference of a factor 1000. A study of 9 different species concentrations for different temperatures and air-fuel ratios is shown in Figure 3.6 and 3.7. The molar fraction of NO is in the order of 0.0005 - 0.1 for temperatures higher than 2000 K. Molar fraction of other main species reach only 0.1-0.7 and can therefore not be the main source for free electrons. This implies that the choice of NO as main contributor is correct under the model assumptions.

3.3 Sensitivity analysis

Temperature affects both the NO formation and the thermal ionization. For modeling the ionization current it is interesting to know how important it is to have accurate models for combustion temperature and NO formation.

Saitzkoff et al. (1996) suggests NO as the main contributor of free electrons through thermal ionization in the post flame phase of the ionization current. Even though the concentrations of NO may be relatively low in the burned mixture, the low ionization energy for NO leads to a high degree of ionization at lower temperatures, see section 3.2. The temperature influence in ionization ratio for NO is showed in Figure 3.8. An increase in temperature from 2200K to 2400K increases the ionization degree by 10 times. A temperature increase also affects the NO generation. Figure 3.2 shows a calculation of NO molar

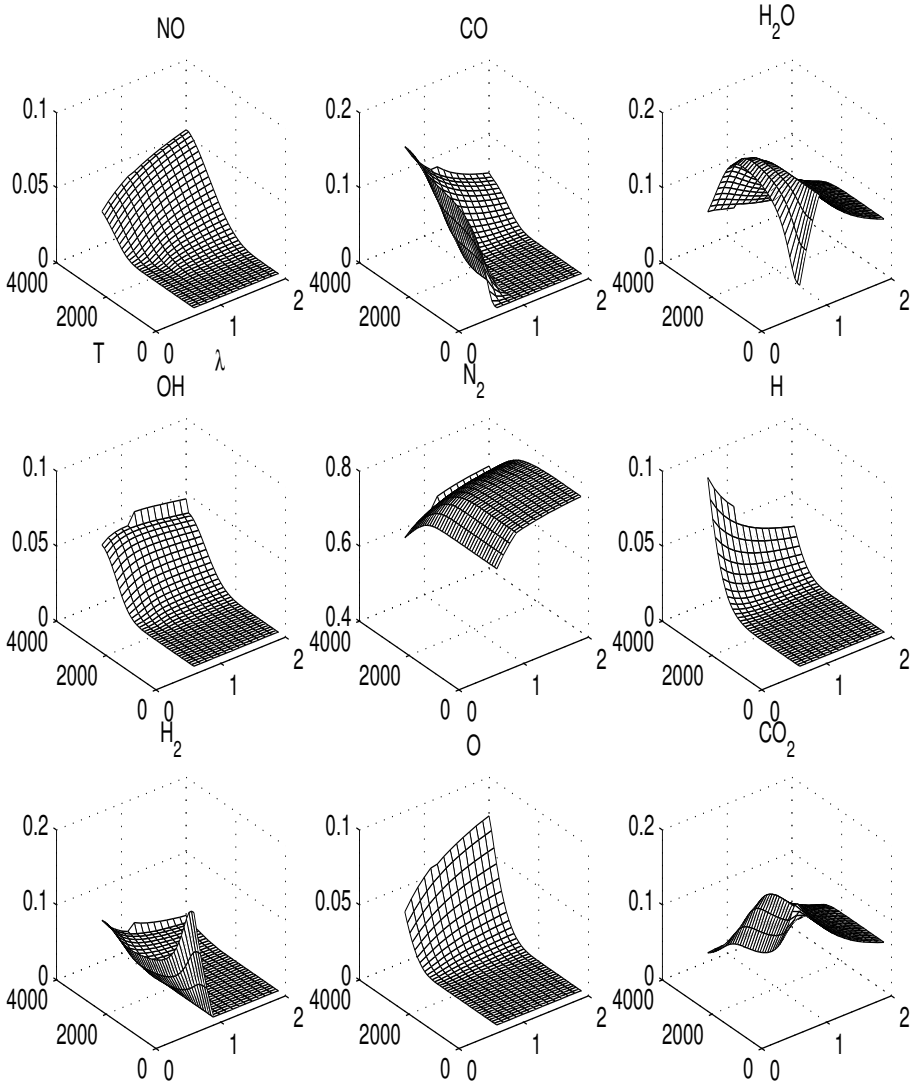

Figure 3.6: *Burned gas composition for different species. Temperature and air-fuel ratio dependency at 20 bar.*

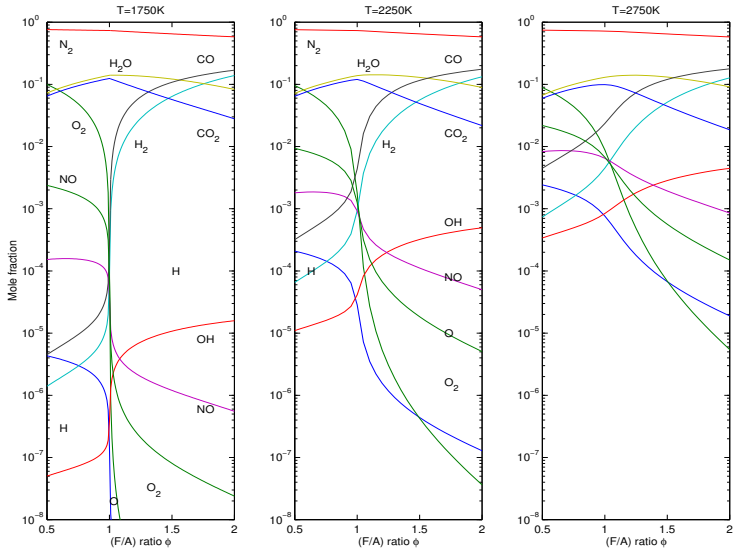

Figure 3.7: *Burned gas composition for different species and air-fuel ratio at 30 bar and 1750 K, 2250 K and 2750 K.*

Figure 3.8: *Ionization ratio dependency on temperature, NO, 20 bar.*

fraction development for different fix temperatures. The end value corresponds to equilibrium conditions. The equilibrium fraction for NO increases 2 times when temperature rises from 2200K to 2400K. However, in a combustion the temperature only stays at the peak level in the order of milliseconds.

Reaction rate limited NO formation is most important for temperatures where the reactions are slow compared to the combustion event, below 2600 K where the characteristic time is 3 ms. For temperatures above 2600 K the reactions are fast and the NO concentration reaches equilibrium. In the range 2600 - 3000 K the NO fraction increases 3 times and the ionization degree 20 times. If the combustion temperature reaches this region the ionization degree dominates over the NO formation. Using a fix level of NO fraction introduces a relatively small error in amplitude. At 1 ms the increase in NO molar fraction is 18 times.

The same analysis for a temperature step from 2400 K to 2600 K gives 10 times ionization degree increase and 2 times NO molar fraction increase at 1 ms. Table 3.4 views how a temperature change impacts on the ionization current.

Temp step	Ionization degree	NO molar fraction	Total ion curr.
2200K - 2400K	×10	×18	42
2400K - 2600K	×10	×2	14

Table 3.4: *Impact of temperature change in ionization current*

First column is the temperature step, the second is the increase in ionization degree, the third is the increase in NO molar fraction at 1 ms and the fourth column is the total increase in ionization current according to the Saitzkoff model. The ionization current model in Equation (2.2) can be simplified to

$$I = A\sqrt{\phi_{NO}}\exp\left[-\frac{E_{NO}}{2kT}\right] \tag{3.11}$$

where I is the current, ϕ_{NO} is the molar fraction of NO in the combusted gas, the exponential factor represents the temperature sensitive part of the ionization degree and A gathers all parts of Equation (2.2) that is not affected by temperature. Actually, one factor in A is $T^{1/4}$ but its impact on I when T changes is negligible compared to the exponential factor.

The ionization current sensitivity differs between the two sources NO molar fraction and ionization degree. The ionization degree comes in linearly but the NO molar fraction comes in as the square root. Both are dependent of temperature and while the ionization degree obviously relates exponentially to the temperature, the NO content relation is not easily unmasked and is investigated with a simple numerical approach instead. The *relative gradients* of NO content and ionization degree with respect to temperature give a measure for the sensitivity.

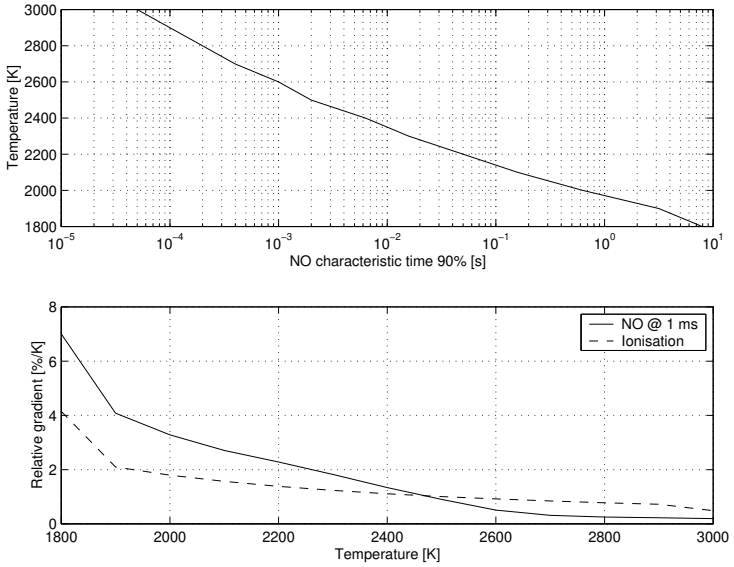

Figure 3.9: *Upper: Characteristic time to reach 90% of equilibrium NO. Lower: Relative NO gradient in temperature*

The relative gradient of a function is defined as the gradient of the function divided by the function value.

$$F_{rel}(f) = \frac{\frac{df}{dx}}{f} \tag{3.12}$$

The relative gradient is a measure for sensitivity. The sensitivity for NO molar fraction with respect to combustion temperature is shown in the lower Figure 3.9. The sensitivity decreases with higher temperature. At 1800 K the NO fraction sensitivity to temperature is 7%/K while the ionization degree sensitivity to temperature is 4%/K. This means that the amplitude of the ionization current changes more due to the change in NO fraction than the change in ionization degree. At higher temperature, >2500 K, the relation is the opposite.

Both NO formation and ionization degree is highly temperature dependent. The choice of combustion temperature is made through the choice of combustion model. The performance of different combustion model approaches will be discussed in the next chapter.

3.4 Conclusions

NO is the most probable of the main combustion product species to be the main source of electrons in the thermal ionization process. The more dominant species

in the combusted gas, CO_2, H_2O and N_2, all have so much higher ionization energy that the total number of ionized particles from these three is much less than from NO. Also, NO has least ionization energy of all species with equal or less concentration than NO.

An extension to the NO formation model presented by Heywood (1988) was developed, that considers the volume change in the burned zone and makes the NO formation model useful in engine cycle calculation.

According to the model presented by Saitzkoff et al. (1996) the amplitude of the ionization current is affected by both NO content and thermal ionization. In the higher temperature region, >2400 K, thermal ionization dominates in sensitivity. In the lower region, <2400 K, the NO formation processes is more important.

4

Temperature models for ionization current description

A combustion model can describe the temperature development in the cylinder. Combustion models may be classified in dimensions and zones. A single-zone model considers the whole combustion chamber to be one zone. A two-zone model divides the combustion chamber in two zones where each zone have its own temperature, volume and mass but share pressure. A zero-dimensional model has no variations in chemical composition, temperature or pressure within each zone. All investigated models in this chapter are zero-dimensional. A multidimensional model is based on fluid dynamics that give information on the flow field in the combustion chamber. This feature can be useful if flame development is modeled. In this case flame development is given via the heat release rate that comes from analysis of pressure data.

The purpose of this chapter is to find a combustion model that describes the combustion temperature in a way that it explains the ionization current. The three different model approaches taken in this chapter are two extremes and one compromise. The two extremes represent the lowest (one-zone) and the highest (kernel zone) possible combustion temperatures from a thermodynamic perspective and the compromise (two-zone) a temperature in between the two extremes. Also, an interesting question is whether a dynamic NO formation model has any impact on the ionization current. Earlier work by Saitzkoff et al. (1996) used a fix NO molar fraction of 1%. This level is supported by the work of Lavoie et al. (1970). The first model upgrade would be to use equilibrium concentrations of NO based on combustion pressure and temperature, and gas composition. However, a reaction rate controlled NO formation process has a property that effects both timing and amplitude of the NO content which may

be useful in the medium temperature area 1800 K to 2400 K. Therefore the equilibrium model step was excluded and the effort was put to investigate the reaction rate controlled NO formation process.

In this case cylinder pressure and cylinder volume are the inputs to the model. The outputs from the model are a combustion temperature trace and the volume of the burned zone. In the case of the one-zone model, the whole cylinder volume is the burned zone.

4.1 One-zone model

A one-zone combustion model considers the whole combustion chamber as one zone and the gas mixture is an ideal gas. This one-zone model represents the lowest possible combustion temperature since the energy released from combustion warms up the whole mixture. The combustion zone volume is equal to the cylinder volume. The gas mass is constant during the whole combustion since blow-by is neglected. The gas constant R can have different level of accuracy. It is calculated as

$$R = \frac{\tilde{R}}{M}$$

where $\tilde{R} = 8,31[J/molK]$ is the universal gas constant and M is the mean molecular weight of the gas mixture. In this case M is a constant. In the case where the cylinder pressure, volume and mass is known, the cylinder temperature is easily derived by the ideal gas law

$$T = \frac{p\,V}{m\,R} \tag{4.1}$$

4.2 Kernel zone model

The highest possible combustion temperature can be reached when the combusted gas is not mixed with any cooler gas. The warmest gas appears in the beginning of combustion if it is allowed to be compressed without heat transfer to the surroundings. The kernel zone model is described as follows.

A small kernel of burned gas is located at the spark plug, as in Figure 4.1. Two assumptions are made about the gas kernel:

1. Burned gas mixing is negligible
2. Heat loss to the surrounding environment is negligible

The kernel of gas is compressed and expanded adiabatically by the surrounding cylinder pressure according to

$$\left(\frac{p}{p_0}\right)^{\frac{\gamma-1}{\gamma}} = \frac{T_k}{T_{k0}}$$

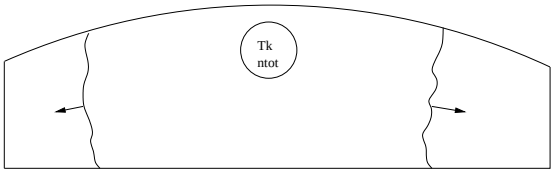

Figure 4.1: *Combustion model for calculation of burned gas temperature close to spark plug.*

where p_0 and T_{k0} are the initial pressure and temperature conditions when the kernel is created, at start of combustion (SOC). The pressure p_0 is trivial, it is equal to the pressure at SOC. The initial temperature T_0 is equal to the temperature of the first burned particles. It is called the adiabatic flame temperature and is calculated by solving the equation:

$$h_r(T_r) = h_p(T_p, p)$$

where h_r and h_p are enthalpy for reactants and products, and T is temperature. The equation means that the internal chemical energy for the reactants is transformed to heat while preserving the pressure constant. The adiabatic flame temperature depends on air-fuel ratio and gas temperature in unburned mixture.

The kernel zone does not exchange any mass with the surrounding zone. The initial kernel temperature is calculated from a linearized model, shown in Figure 4.2. The adiabatic flame temperature T_0 is modeled as a function of air fuel ratio and initial gas temperature. T_0 is calculated as

$$T_{k0} = T_a(\lambda) + T_a(T_{init}) - T_a(293K) \tag{4.2}$$

where it is assumed that the contribution from a change in initial temperature is independent of air-fuel ratio.

Heat loss and residual gases are not considered in this model. Heat loss will reduce the peak temperature and residual gas reduces the flame temperature. One simple way to account for these effects is to reduce the initial temperature T_0, which then becomes a calibration parameter. This method was used by Saitzkoff et al. (1996).

4.3 Two-zone model

A two-zone model is characterized by the two, fully mixed zones, one composed by burned gases and one by unburned gases. The two zones are separated by an infinitesimal thin divider representing the flame front. Within each zone the mixture is homogeneous with respect to temperature and chemical composition.

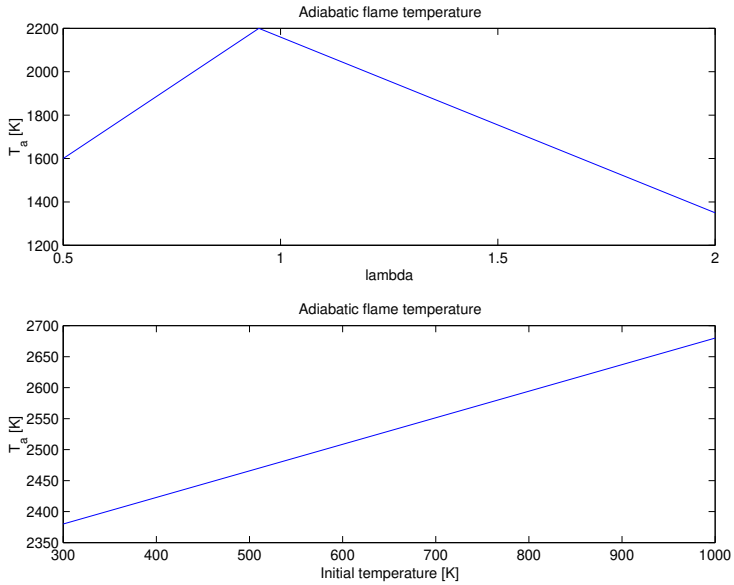

Figure 4.2: *Adiabatic flame temperature as a function of a) λ at initial temperature 293 K, b) initial temperature at $\lambda = 1$.* The model is simplified to a linear relation.

Both zones share pressure since the divider is soft and moves to equalize the pressure on both sides. A fraction of mass dm_{ub} enters the burned zone with enthalpy h_{ub} as the combustion proceeds and adds the energy $dm_{ub}h_{ub}$ to the total burned zone energy U_b. The burned zone expands and the unburned zone is compressed. The burned zone looses energy $p\,dV_b$ in the expansion work. The process is described by the following equation:

$$dU_b = -p\,dV_b + dm_{ub}h_{ub} \tag{4.3}$$

A central part for two-zone models is the calculation of the mass entering the burned zone dm_{ub}. This part is here given certain attention before solutions to Equation (4.3) is discussed.

Two approaches for calculating burned zone temperature were investigated. The first approach is based on state-of-the-art two-zone thermo-dynamical modeling, presented by Nilsson and Eriksson (2001). However, this method showed numerical problems in solving the differential equation due to noise in the input signals. Since the purpose is to get a temperature in between the two extremes, rather than the most exact two-zone temperature, another method was developed. This method is more based on common sense assumptions about cylinder temperatures than thermodynamic modeling of the mass transport between the two zones. The second method is called *temperature mean value approach*.

Burned mass fraction

Krieger and Borman (1966) described a method of calculating heat release rate from cylinder pressure and volume. A simplified model that does not consider losses is

$$\frac{dQ}{d\theta} = \frac{\gamma}{\gamma - 1}p\frac{dV}{d\theta} + \frac{1}{\gamma - 1}V\frac{dp}{d\theta} \tag{4.4}$$

where dQ is the heat release rate, θ is crank angle, γ is the polytropic exponent for the adiabatic process of compression and expansion, p is the cylinder pressure and V is the cylinder volume. The accumulated released energy from combustion at any crank angle is $Q(\theta)$:

$$Q(\theta) = \int_{SOC}^{\theta} dQ(\theta) \tag{4.5}$$

The burned mass fraction mfb is defined as

$$mfb(\theta) = \frac{m_b(\theta)}{m_{tot}} \tag{4.6}$$

where m_b is the mass of the burned gas and m_{tot} is the total mass of the gas in the cylinder. An assumption is made that the heat release reflects the actual burned mass. The burned mass fraction can then be calculated as

$$mfb(\theta) = \frac{m_b(\theta)}{m_{tot}} = \frac{Q(\theta)}{Q_{max}} \tag{4.7}$$

Two-zone model: Nilsson and Eriksson approach

Nilsson and Eriksson (2001) described a new way to formulate a two-zone model. A simplified version of their model is used here, where no heat loss is considered. The model is described as a differential algebraic equation

$$\mathbf{A}dx = \mathbf{B} \tag{4.8}$$

where the differentials of the states are

$$dx = \begin{pmatrix} dp \\ dV_1 \\ dT_1 \\ dV_2 \\ dT_2 \end{pmatrix}$$

$$\mathbf{A} = \begin{pmatrix} 0 & 1 & 0 & 1 & 0 \\ a_1 & p & b_1 & 0 & 0 \\ c_1 & p & d_1 & 0 & 0 \\ a_2 & 0 & 0 & p & b_2 \\ c_2 & 0 & 0 & p & d_2 \end{pmatrix}$$

$$\mathbf{B} = \begin{pmatrix} dV \\ R_1 T_1 dm_{12} \\ (h_{12} - h_1 + R_1 T_1) dm_{12} \\ -R_2 T_2 dm_{12} \\ -(h_{21} - h_2 + R_2 T_2) dm_{12} \end{pmatrix}$$

$$\begin{aligned} a_i &= V_i \\ b_i &= -m_i R_i \\ c_i &= 0 \\ d_i &= m_i (c_p - R_i) \end{aligned}$$

Unburned zone is denoted 1 and burned zone is 2. The choice of constants a to d use the assumption that R is constant and not dependent of changes in temperature or pressure. This model use the burned mass rate dm_{12} and cylinder volume as inputs and calculates volume and temperature for each zone and the global pressure. The burned mass fraction was calculated from the measured pressure trace using Equation (4.7)

The Equation system (4.8) has one unique solution and gives the differential of the state for any input combination. The solution to the differential equation system is obtained by a numerical method. One problem here is if the input

burned mass rate dm_{12} contain some noise. This will affect the calculation of the states. Noise can be interpreted as a reversed combustion, and this is especially crucial when one zone is very small. The state of small zones can take unreasonable values, e.g. negative temperature, volume or mass.

If the cylinder pressure is known it can be used in the model as input. The first column in matrix $\mathbf{A}$ times dp is moved to column array $\mathbf{B}$. The new system is now over-determined and the reduced state-differential array

$$dx = \begin{pmatrix} dV_1 \\ dT_1 \\ dV_2 \\ dT_2 \end{pmatrix}$$

is calculated as the LMSE solution to equation system (4.8). The same problem arises with noise in dm_{12}. The noise is now present in both the burned mass fraction and the cylinder pressure.

Temperature mean value approach

A more simplified temperature model is based on a single-zone combustion model and adiabatic compression of the unburned mixture. The single-zone model temperature can be seen as a mean value of the two zone temperatures in a two-zone model, weighted by mass in each zone. The procedure in this method is as follows:

1. calculate the single-zone temperature as in Equation (4.1)
2. calculate the unburned zone temperature in a two-zone model
3. calculate the heat release rate, Equation (4.4)
4. calculate burned zone temperature

Each part of the unburned mixture is only affected by the total cylinder pressure before the combustion occurs. The unburned zone temperature is referenced to a point where pressure and temperature is known.

$$T_u = T_{u,SOC} \left(\frac{p}{p_{SOC}} \right)^{\frac{\gamma-1}{\gamma}} \tag{4.9}$$

Conditions at start of combustion, SOC, can be estimated from conditions at intake valve closing, IVC. The gas mixture captured in the cylinder is compressed in an adiabatic process forming the motored temperature T_m:

$$T_m = T_{IVC} \left(\frac{V_{IVC}}{V} \right)^{\gamma-1} \tag{4.10}$$

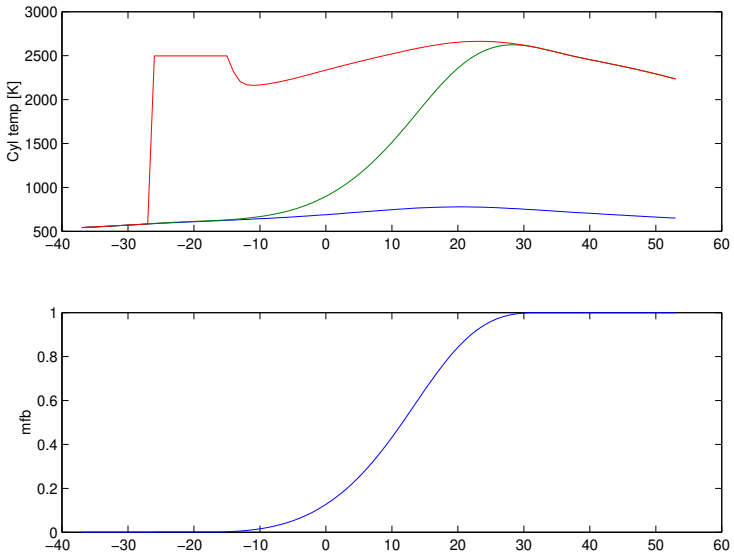

Figure 4.3: *Zone temperatures and burned mass fraction for the temperature mean value 2-zone model*

The unburned zone shares the properties of the motored temperature at SOC.

$$T_{u,SOC} = T_{m,SOC} \tag{4.11}$$

The burned mass fraction is calculated by Equation (4.7) The single-zone temperature T_{1zone} is calculated as Equation (4.1) and is seen as the mass-weighted mean temperature of the two zones

$$T_{1zone} = \frac{m_b T_b + m_u T_u}{m_b + m_u} \tag{4.12}$$

In this case the difference in specific heat capacity c_v is neglected. Including a model for c_v would increase the importance of the burned gas temperature T_b. Equation (4.12) gives T_b as

$$T_b = T_{1zone}(1 + \frac{m_u}{m_b}) - T_u \frac{m_u}{m_b} \tag{4.13}$$

The calculation of T_b is sensitive for low values of the burned mass fraction, mfb. As seen in Figure 4.3 the temperature calculation is unreliable for mfb < 0.01. In this case a temperature limitation of 2500 K, the adiabatic flame temperature, was set for mfb < 0.01. The reason for the unreliability is that mfb and T_{1zone} is calculated independently from each other, with no assumptions of T_b.

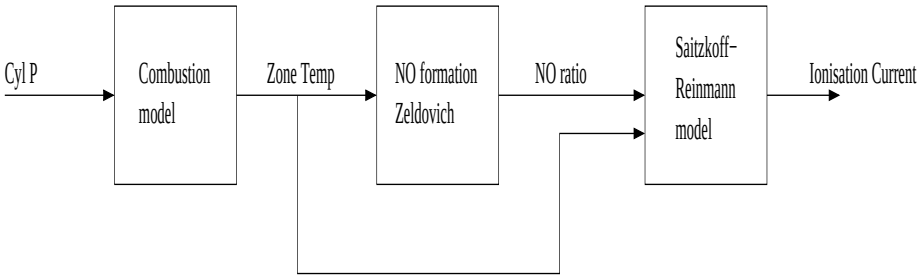

Figure 4.4: *A view of the simulation process.*

The burned zone volume, V_b, is calculated as

$$V_b = \frac{T_b \,\mathrm{mfb}}{\mathrm{mfb}\, T_b + (1 - \mathrm{mfb}) T_u} V \tag{4.14}$$

where V is the total cylinder volume.

4.4 Temperature model evaluation

The temperature models are here evaluated in the point of view of how they explain the ionization current, assuming thermal ionization. To do that a simulation model was designed according to Figure 4.4.

Simulation of ionization currents are based on pressure traces. A chain of calculations will finally lead to the ionization current as in Figure 4.4. A combustion model uses the pressure trace to calculate the temperature for the burned gases of interest. Both the NO formation calculation and the ionization current simulation then use the temperature trace.

Section 3.2 summarizes the model presented by Saitzkoff et al. (1996), for thermal ionization of nitric oxide, NO. This model is based on the assumption that the main carriers are free electrons. The main generator for free electrons is the thermal ionization of nitric oxide. The model for the ionization current looks like

$$I = U \frac{\pi r^2}{d} \frac{e^2}{\sigma m_e \sqrt{\frac{8kT}{\pi m_e}}} \sqrt{\phi_s} \sqrt{\frac{2\left(\frac{2\pi m_e kT}{h^2}\right)^{\frac{3}{2}} \frac{B_1}{B_0} \exp\left[-\frac{E_1}{kT}\right]}{n_{tot}}}$$

where the parameters are listed in Table 4.1.

In this model there are three variables that are crank angle dependent; temperature T, particle density n_{tot} and molar fraction of NO ϕ_s. Saitzkoff et al. (1996) made simulations based on a kernel-zone model and a fixed NO molar

U	spark gap voltage
r	radius of measurement cylinder
d	length of measurement cylinder
e	unit charge constant
σ	collision cross section
m_e	electron mass
k	Bolzmann's constant
T	temperature of gas
ϕ_s	number density of NO
h	Planck's constant
B	internal partition function
E_1	ionization energy for first order ionization
n_{tot}	total number density of particles in ionization process

Table 4.1: *Model parameters of ionization current model, (Saitzkoff et al., 1996)*

U	80 V
r	1 mm
d	1 mm
σ	0.1 Å^2
m_e	9.31e-31 kg
$\frac{B_1}{B_0}$	1
E_1	9.25 eV
k	1.38e-23 J/K
h	6.63-34 Js
e	1.6 e-19 As

Table 4.2: *Parameter values in Saitzkoff-Reinmann model*

fraction. The constant parameters of the model were set to values according to Table 4.2.

The three combustion models and the choice of static or dynamic NO formation presents six combinations for ionization current simulation. They are all presented to show the importance of model choice.

Engine data used

The evaluation data consists of pressure traces from 50 cycles at 2000 rpm and 100 Nm and stoichiometric air fuel mixture. The result for each method is presented with a plot of one combustion cycle from the data set, the same cycle for all methods, just to illustrate the behavior. In the summary a table presents the result from all cycles in the data set.

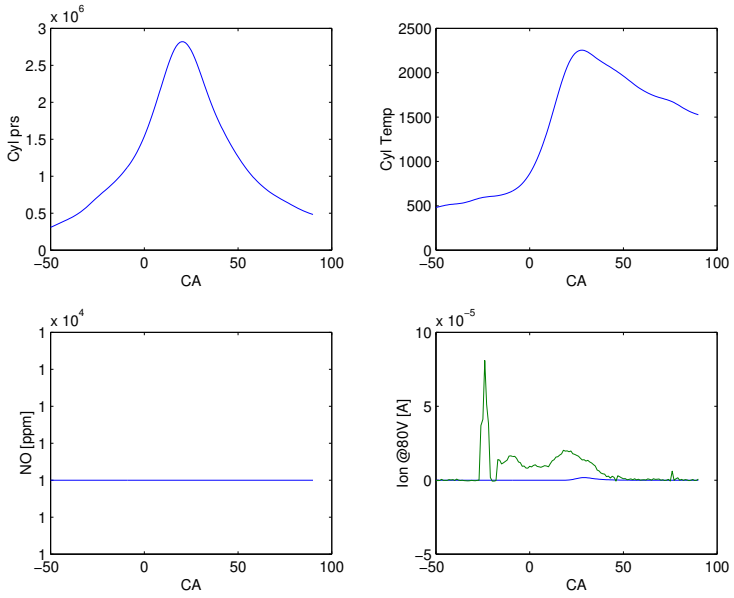

Figure 4.5: *Simulation result from a one-zone, fix NO content.*

4.4.1 Results from one-zone, fix NO model

The measured cylinder pressure and the volume function were used for calculating the cylinder temperature in the one-zone model. A fix content of NO was used, 1% molar fraction. The total output of cylinder temperature, NO and pressure were used for ionization current simulation. Figure 4.5 shows the result. The upper left graph is cylinder pressure, the upper right is one-zone temperature, the lower left is NO molar fraction and the lower right shows the calculated ionization current compared to the actual measured current. Combustion temperature reach 2250 K in peak value and NO molar fraction is 10000 ppm. The calculated current is only 1/16 of the actual measured current and not visible in the plot. The position of the peak of the simulated ionization current appears at 29 CAD, the same angle as the temperature peak, which is 11 CAD later than the measured current.

4.4.2 Results from one-zone, dynamic NO model

The measured cylinder pressure and the volume function were used for calculating the cylinder temperature in the one-zone model. The generated temperature trace was used for rate-controlled NO calculations and the total output of cylinder temperature, NO and pressure were used for ionization current simulation. Figure 4.6 shows the result. The upper left graph is cylinder pressure, the upper

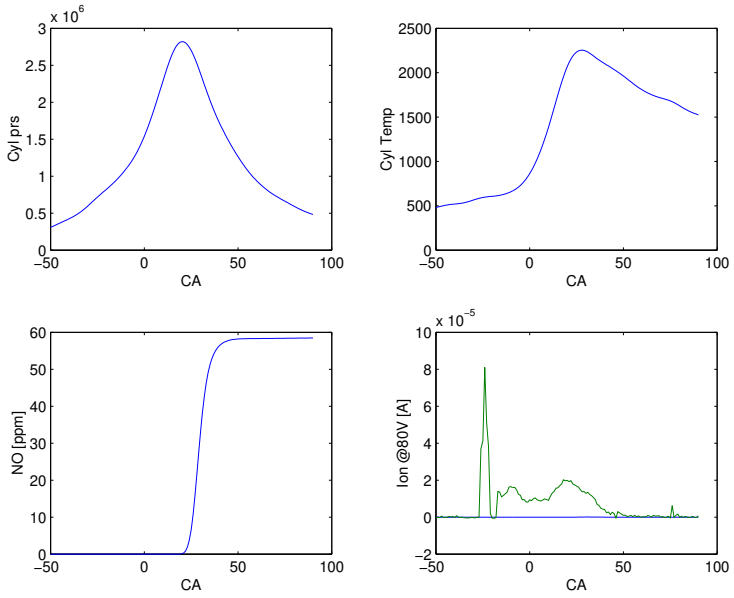

Figure 4.6: *Simulation result from a one-zone, dynamic NO model.*

right is one-zone temperature, the lower left is calculated NO molar fraction and the lower right shows the calculated ionization current compared to the actual measured current. Combustion temperature reach 2250 K in peak value and NO content peaks at 60 ppm. The calculated current is only 1/350 of the actual measured current and not visible in the plot. The position of the peak of the simulated ionization current appears at 31 CAD which is 11 CAD later than the measured current.

The low combustion temperature produced by the one-zone model generate both low concentrations of NO and low ionization degree. Calculations done by Lavoie et al. (1970) show that a normal content of NO is in the region of 1% during combustion at stoichiometric air-fuel ratio.

4.4.3 Results from kernel zone, fixed NO model

Using the kernel-zone combustion model for temperature calculations and a fixed concentration for NO_x a simulation of second peak may look like Figure 4.7. The result is dependent of the set of parameters viewed in Table 4.2.

Peak temperature reach just over 3000 K and NO molar fraction is fixed at 1%. The resulting ionization current is in the order of 50 times higher than the measured current and 800 times higher than the one-zone fix NO case. The main source for the increase is the higher ionization degree. The peak position

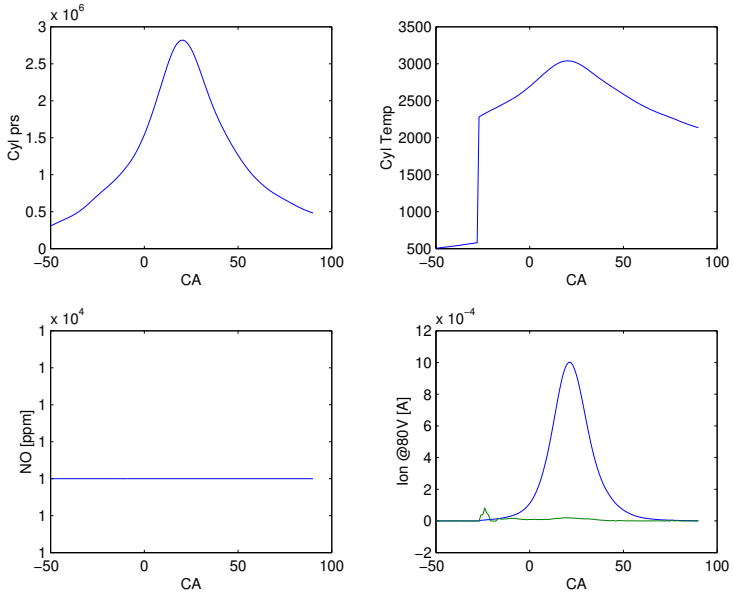

Figure 4.7: *Simulated ionization current using the kernel combustion model and a fixed molar fraction of NO*

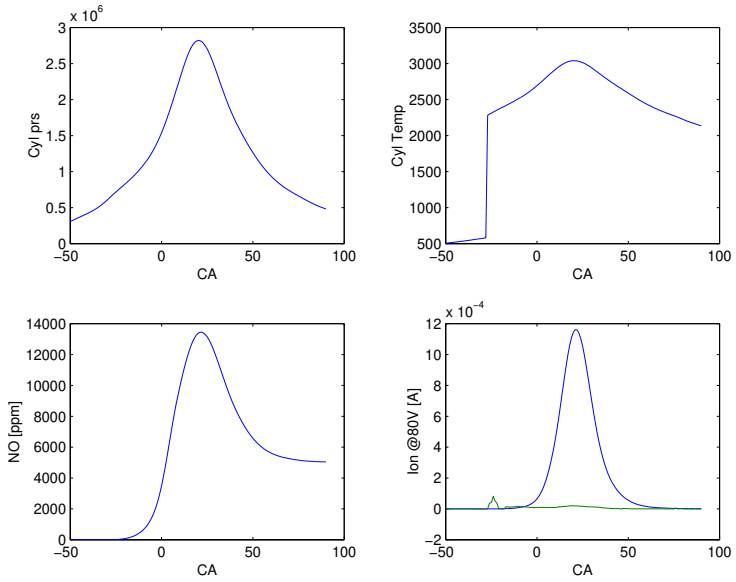

Figure 4.8: *Simulation of ionization current from SAAB 9000 engine data. Simulated current is compared to the measured current.*

of the current is at 21.5 CAD which is only 1.5 CAD later than the measured current peak.

4.4.4 Results from kernel zone, dynamic NO concentration model

The combustion model calculates, as before, the temperature development in a control volume close to the spark plug. The NO formation model gives a concentration of NO from the temperature and pressure conditions in the control volume. Saitzkoff-Reinmann model calculates the ionization ratio and the modeled ionization current.

The result is viewed in Figure 4.8. Peak temperature reach just over 3000 K and NO content peaks at 13500 ppm. The high temperature increases the NO concentration by 200 times compared to the one-zone simulation. The resulting ionization current is in the order of 350 times higher than the measured current and 35000 times higher than the one-zone case. The peak position of the current is the same as for the kernel zone fix NO case, 1.5 degree later than the measured current. The position is nor affected by the dynamic NO formation since the peak temperature is high enough for the reactions to reach equilibrium. Compared to the fixed NO concentration case the amplitude increase is low, only 15%. That is in line with the model since ionization current is affected

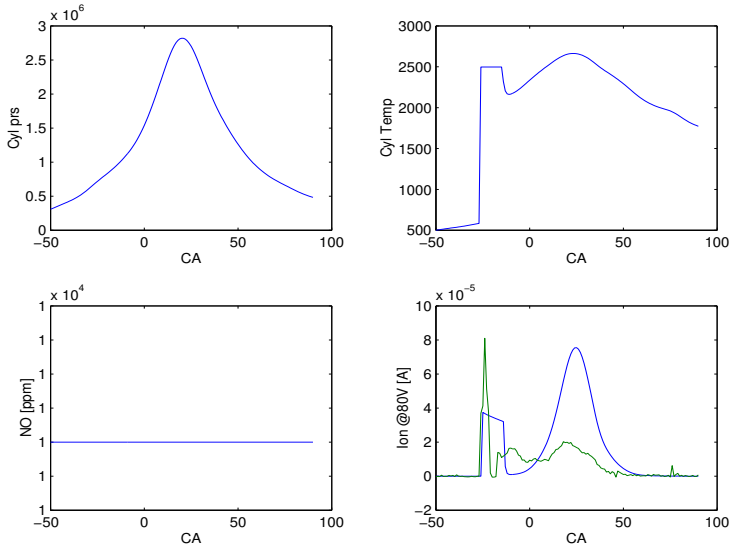

Figure 4.9: *Simulated ionization current using the two-zone combustion model and a fixed molar fraction of NO*

by the square root of NO concentration, and that the ionization degree due to temperature is the same.

4.4.5 Results from two-zone, fixed NO model

Using the two-zone combustion model described in Section 4.3 for temperature calculations and a fixed concentration for NO_x a simulation of second peak may look like Figure 4.9. The result is presented in Figure 4.9. The NO content was set to 1%:

ϕ_s	0.01

The cylinder temperature reaches maximum 2700 K. The early phase of combustion show difficulties in calculation. Between -25 and -10 CAD the temperature calculation is very unstable and was in this case limited to 2500 K for viewing purposes. This part is not interesting from an ionization current point of view and the resulting simulated ionization current in this angle window has no correspondence to the reality. The important part comes between 0 and 100 CAD. The amplitude of the simulated current is now more in the same region as the actual current, only 4 times higher. The peak of the simulated current occurs at 24 CAD ATDC, which is 4 CAD later than the measured current.

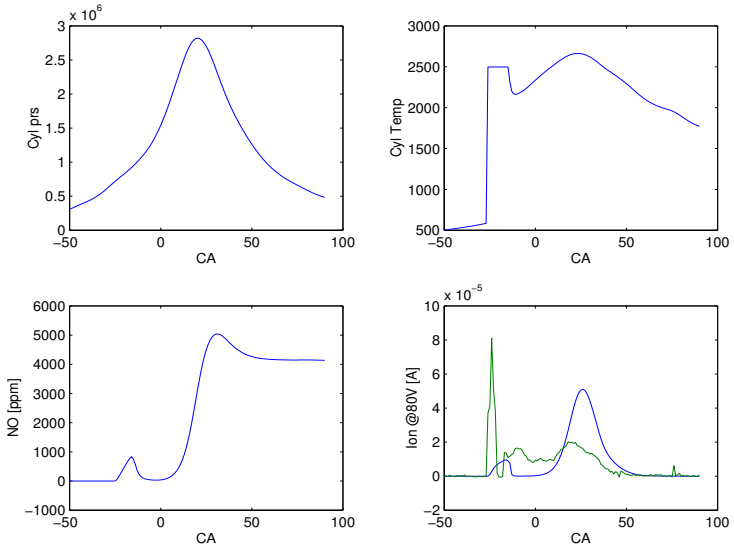

Figure 4.10: *Simulation of ionization current from SAAB 9000 engine data. Simulated current is compared to the measured current.*

4.4.6 Results from two-zone, dynamic NO concentration model

The two-zone combustion model in Section 4.3 calculates, as before, the temperature development in the burned zone. The NO formation model gives a concentration of NO from the temperature and pressure conditions in the control volume. The Saitzkoff-Reinmann model calculates the ionization ratio and the ionization current. The result is presented in Figure 4.10. In this case the temperature is the exact same as in Figure 4.9 but the NO formation is different. The temperature is not high enough to produce 1% NO, maximum reaches 0,5%. The lower ratio of NO reduces the ionization amplitude to 2,5 times higher than the actual current. The position of the simulated ionization current is also affected. The peak occurs at 26 CAD ATDC which is 6 CAD later than the measured current. The shift in peak position appears since the NO content is still increasing when the temperature peak occurs. The temperature peak is located at 24 CAD ATDC.

4.5 Model discussion and conclusions

The one-zone and the kernel combustion models represent two extremes of combustion temperature models. The one-zone model with its fully mixed combustion produces the lower limit of combustion temperature which also is seen in

the simulated ionization current. The amplitude of the simulated current is only a few percent of the actual measured one. The kernel model on the other hand, with its non-mixed burned gas kernel produces the upper limit of combustion temperature. The amplitude of the simulated current is now some 50 times higher than the measured one. The two-zone model represents a middle course between the two extremes.

The interest in the measured ionization current is focused on the second peak which is modeled to be caused by thermal ionization of NO. The peak value is located at 20 CAD ATDC and the amplitude is maximum 20 μA. A summary of the simulation results based on the single reference cycle is listed in Table 4.3.

Method	**Relative amplitude**	**Position [CAD ATDC]**	**max temp [K]**
Measured	1	20	-
1-zone fix NO	1/16	29	2250
1-zone dyn NO	1/350	31	2250
kernel zone fix NO	50	21,5	3000
kernel zone dyn NO	60	21,5	3000
2-zone fix NO	4	24	2700
2-zone dyn NO	2,5	26	2700

Table 4.3: *Summary of simulation results based on one reference cycle*

The analysis was extended to cover all cycles in the data set. Table 4.4 shows the summary of that analysis. The amplitude and peak position is the mean value of all cycles in the data set. The mean value of the peak position of the measured ionization current is located at 16 CAD ATDC and the amplitude is maximum 12 μA.

Method	**Relative amplitude**	**Position [CAD ATDC]**	**max temp [K]**
Measured	1	16	-
1-zone fix NO	1/5	25	2275
1-zone dyn NO	1/202	23	2275
kernel zone fix NO	42	18	2950
kernel zone dyn NO	48	18	2950
2-zone fix NO	1/2	19	2360
2-zone dyn NO	1/20	21	2360

Table 4.4: *Summary of simulation results from all cycles in data set. 2000 rpm, 100 Nm, λ=1*

The one-zone models do not fit the ionization model at all. The amplitude

is only a few percent of the actual and the position is about 8 CAD late. The kernel zone models present a high amplitude but the position is good, only 2 CAD difference. The two-zone models present an amplitude that is slightly low and a position that is later than the kernel model, 4 CAD from the measured current. By adjusting parameters in the thermal ionization model within physically reasonable ranges it is possible to come closer to the actual amplitude level. For example, if the radius r of the measurement cylinder increases from 1 to 1.5 mm, the amplitude increases 2.25 times.

Adding the dynamic NO formation process does not apparently improve the model for one operating point since the same correction can be achieved through parameter calibration. However, I believe that the dynamic NO formation modeling can contribute to a better model agreement when the operating point is changed, e.g. for lean operation when the combustion temperature will decrease and the formation process of NO gets more important.

The investigation shows how important the temperature model is for modeling the ionization current. The temperature has large impact on both NO content and ionization ratio. Earlier measurements done by Greenhalgh (1983) points at combustion peak temperatures of 2700-2800 K for stoichiometric to slightly rich operation. Lean operation decreases the combustion temperature. A combustion model that finds a peak temperature between the kernel model and the two-zone model will both explain the combustion itself better and produce an ionization current amplitude which is closer to the measurements.

5

A novel cylinder pressure model

More complex engine designs are continously being considered and developed. To manage the increased complexity the traditional engine control designs that are based on calibrated maps will require much development time. Here the model based techniques can play an important role since the models provide the couplings between inputs, outputs, and parameters and have the potential to reduce calibration time. Cylinder pressure traces contain information about the work and emission producing process which is valuable for the engine management system. For some diagnosis and control problems it would be beneficial to have information about the cylinder pressure available, some examples are spark advance control, estimation of torque generation, and misfire detection.

Current cylinder pressure models are computationally demanding and it is not yet possible to simulate or to have an observer for the cylinder pressure online in conventional engine control units. Therefore computationally simple models for cylinder pressure in combustion engines are tractable for control purposes. Here an analytical model is developed and validated for the cylinder pressure of a spark ignited (SI) engine, which is computationally tractable since it does not require a numerical solution of the ordinary differential equations, and can thus be used on-line. Work in this direction has already been made for diesel engines by Allmendinger et al. (2001) where the differential equation for the cylinder temperature is reduced to an Riccati differential equation that is solved analytically.

One of the key ideas behind the model here is based on the observation that the ideal Otto cycle provides valuable information about the compression and

expansion processes. These two processes are seen in the real measured pressure traces under normal operating conditions as the asymptotes before the ignition and after the combustion is finished. The real cycle is similar to the ideal Otto cycle and the similarities are largest early in the compression and late in the expansion. It is characterized by the compression and expansion phases which are well defined by the states of the fluid. The second key idea is that the heat release analysis procedure based on pressure ratio management, developed by Matekunas (Matekunas, 1986, 1984, 1983), gives a good approximation of the heat release trace. This method can easily be inverted and used to interpolate between the compression and expansion trace.

The model is described using measurements readily available in production engines and using a set of tuning parameters that have physical interpretations and are closely connected to the ideal Otto cycle. This work focuses on investigating the accuracy of the simple model, not on how parameters can be determined or predicted. The interesting question is, how well the simple model describes the in-cylinder pressure during the high pressure and combustion phase. The burn rate of the combustion has a big influence on the pressure and in the validation the burn rate is considered to be known. However, there are several approaches presented for estimating the burn rate which could be used directly in this model. Two slightly different approaches are described by Csallner (1980); Hires et al. (1978) that present ways of predicting the variations of the burn angles over the full engine operating range by utilizing a reference measurement in a central area of the operating point. Another approach is described by Daniels (1998) which is based on the ionization current measurements, this approach is also applicable since the ion current has been used in production cars since 1994, see e.g. Auzins et al. (1995).

5.1 Model description

Figure 5.1 outlines the ideas behind and the structure within the model. The modeled pressure trace $p(\theta)$ is built up by two asymptotic traces and an interpolation between these. The cylinder pressure model is divided into four parts:

- The compression process is well described by a polytropic process. The polytropic process also encapsulates the heat transfer, so that there is no need to explicitly include the heat transfer in the model.
- The expansion asymptote is also well described by a polytropic process. The reference point for expansion temperature and pressure is calculated using a constant-volume combustion process.
- The concept of pressure ratio management provides a convenient way to interpolate from compression to expansion. Its appearance is very close to the mass fraction burned profile and the Vibe function is used to describe the pressure ratio.

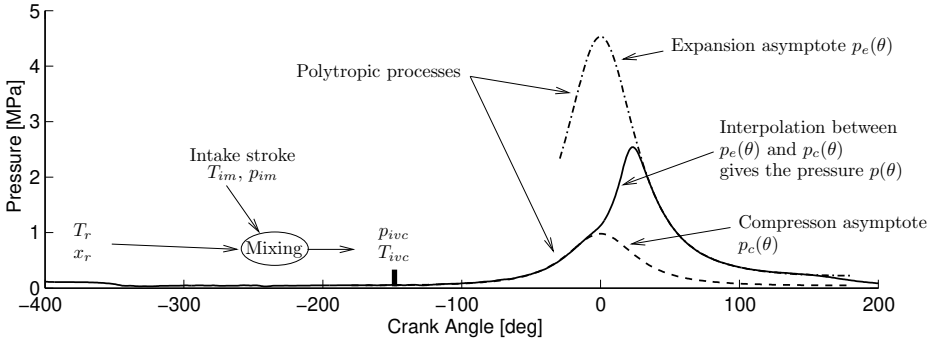

Figure 5.1: *The model is based on the compression pressure, the expansion asymptote, and an interpolation between these. Initial conditions are determined from the intake conditions and the residual gases.*

- Gas exchange phase. During the period IVO-IVC the pressure is approximated by the intake manifold pressure. During the period EVO-EVC the pressure is approximated by the exhaust manifold pressure. Between the phases the pressure can be determined through an interpolation using for example a cosine function.

5.1.1 Compression part in the cycle

It is a well known fact that the compression process can be modeled with good accuracy by a polytropic process. Such a process is described by a polytropic exponent k_c and a value at one reference point. One point that can be used as reference is the intake valve closing (IVC) which gives the following expressions for the compression pressure and temperature

$$p_c(\theta) = p_{ivc} \left(\frac{V_{ivc}}{V(\theta)} \right)^{k_c} \tag{5.1}$$

$$T_c(\theta) = T_{ivc} \left(\frac{V_{ivc}}{V(\theta)} \right)^{k_c - 1} \tag{5.2}$$

These traces describe the cylinder pressure and temperature up to the point of ignition. The temperature model is also necessary to have in this approach since it has a direct impact on the second pressure asymptote.

Determination of initial pressure

The manifold pressure gives a good indication of the initial pressure for the compression stroke. However pressure drops over valves as well as tuning effects in the intake runners also have an influence. Here a reference condition just

before IVC is used to determine the initial pressure

$$p_{ivc} = p_{im}(\theta_{ivc})$$

The crank angle for intake valve closing θ_{ivc} is not exactly known due to production tolerances, it is also used as tuning parameter to compensate for pressure drops over the valves etc. Additionally an affine correction in engine speed is tested which improves the accuracy of the compression pressure model slightly,

$$p_{ivc} = p_{im}(\theta_{ivc}) + c_1 + c_2 * N$$

Here c_1 and c_2 are parameters that have to be determined which increases the flexibility but also the model complexity. To maintain simplicity the evaluation is concentrated on the first model.

Determination of initial temperature

It is more difficult to determine the fluid temperature at intake valve closing compared to the pressure, since it is influenced by heat transfer and residual gases that are difficult to measure and determine. The air in the intake manifold is heated from T_{im} to T_a by the hot valves and the locally high heat transfer coefficients in the cylinder. Fuel is added in the ports and undergoes an evaporation which also influences the temperature. By considering the energy equation with a lumped process for heating, evaporation, and mixing, the initial air/fuel mixture temperature can be stated as

$$T_{af} = \frac{m_a\, c_{p,a}\, T_a + m_f\, c_{p,f}\, T_f - m_f\, h_{v,f} + Q}{m_a\, c_{p,a} + m_f\, c_{p,f}}$$

where $h_{v,f}$ is the vaporization enthalpy for the fuel and Q is the heat added to the fresh mixture. Both these are difficult to determine. In the cylinder the fresh charge is mixed with the residual gases and the mixture temperature is

$$T_{ivc} = \frac{m_{af}\, c_{p,af}\, T_{af} - m_r\, c_{p,r}\, T_r}{m_{af}\, c_{p,af} - m_r\, c_{p,r}}$$

Prior to mixing the residual gases are cooled down by heat transfer to the walls.

Simplifying the temperature model

The outlined models for heating, evaporation, and mixing processes are complex and contain several variables that have to be determined. The central question here is to see how well a simple model can capture the process and therefore some simplifications are made. First it is assumed that the specific heats c_p are the same for the residual gas and the fresh air and fuel mixture yields

$$T_{ivc} = T_{af}\,(1 - x_r) + x_r\, T_r \tag{5.3}$$

where the residual gas fraction is defined as

$$x_r = \frac{m_r}{m_a + m_f + m_r}$$

The heat transfer to the fresh fluid is also neglected and the fresh fluid is set equal to the temperature in the intake manifold,

$$T_{af} = T_{im}$$

Finally the heat transfer from the residual gas is neglected and the residual gas temperature T_r is set equal to the temperature at the end of the cycle. This approach is mainly justified by its simplicity, but there are some effects that cancels out, e.g. the heat transfer to the fresh mixture and the heat transfer from the residual gases are both neglected and cancels some of the effects of each other. The residual gas fraction x_r is maintained constant but better estimates can be received from an ideal Otto cycle, using for example one of the procedures outlined by Heywood (1988) or Mladek and Guzzella (2000).

5.1.2 Asymptotic final pressure

The asymptotic expansion process is also modeled as polytropic, with polytropic exponent k_e

$$p_e(\theta) = p_3 \left(\frac{V_3}{V(\theta)} \right)^{k_e} \tag{5.4}$$

$$T_e(\theta) = T_3 \left(\frac{V_3}{V(\theta)} \right)^{k_e - 1} \tag{5.5}$$

The determination of V_3, p_3, and T_3, that refer to state three in the ideal Otto cycle, will be discussed below, see Figure 5.2. The pressure p_3 can be determined experimentally by inverting the pressure ratio analysis (Matekunas, 1986, 1984, 1983). Here a constructive approach is presented it is based on the ideal Otto cycle that accounts for the physical properties in the system. Air-to-fuel ratio and ignition timing both have an influence on the final pressure and these are covered by this approach

From state 2 to state 3 in the pV diagram, see Figure 5.2, the temperature increase is determined by,

$$\Delta T_{comb} = \frac{m_f \, q_{HV} \, \eta_f(\lambda)}{c_v \, m_{tot}} = \frac{(1 - x_r) \, q_{HV} \, \eta_f(\lambda)}{(\lambda (A/F)_s + 1) \, c_v} \tag{5.6}$$

the fuel conversion efficiency $\eta_f(\lambda)$ comes from Figure 3.9 in Heywood (1988) and the following expression is used

$$\eta_f(\lambda) = 0.95 \, min(1;\, 1.2\lambda - 0.2)$$

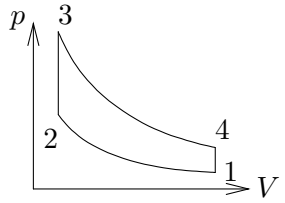

Figure 5.2: *Sketch of the ideal Otto cycle that defines the states 2 and 3.*

For a thorough discussion of the ideal cycle see e.g. Chapter 5 in (Heywood, 1988). The equation takes the effect of varying air-to-fuel ratios by considering the effect that the fuel mass has on the temperature increase. Exhaust gas recirculation EGR can also be included, this enters the equations in the same way as the residual gas and influences both the initial temperature T_{ivc} and the dilution x_r. In the evaluation the thermodynamic properties of the fluids (i.e. c_v, k_c and k_e of burned and unburned gases) are considered to be independent of λ which is a simplification.

The temperature after the combustion becomes

$$T_3 = T_2 + \Delta T_{comb}$$

Finally the pressure after the combustion is determined from the ideal gas law

$$p_3 = p_2 \frac{T_3}{T_2} \tag{5.7}$$

where p_2 and T_2 are determined from Equations ((5.1)) and ((5.2)).

Method to account for combustion phasing

Ignition timing and combustion phasing influence the final pressure, see Figure 5.3. This is taken into account by phasing the ideal Otto combustion in a special way using the mass fraction burned trace. The position for the combustion θ_c is chosen to be at TDC if the calculated position for 50% mass fraction burned, mfb_{50}, is at its optimal value, $MFB_{50,OPT}$. If the mfb_{50} position deviates from its optimum, the angle θ_c is set to that deviation in CAD.

$$\begin{aligned} \theta_c &= mfb_{50} - MFB_{50,OPT} \\ mfb_{50} &= \Delta\theta_d + \frac{1}{2}\Delta\theta_b \\ MFB_{50,OPT} &= 0^\circ\text{ATDC} \end{aligned}$$

where the optimal value for the 50% mass fraction burned is set to 0°. The model above is motivated by the following observations:

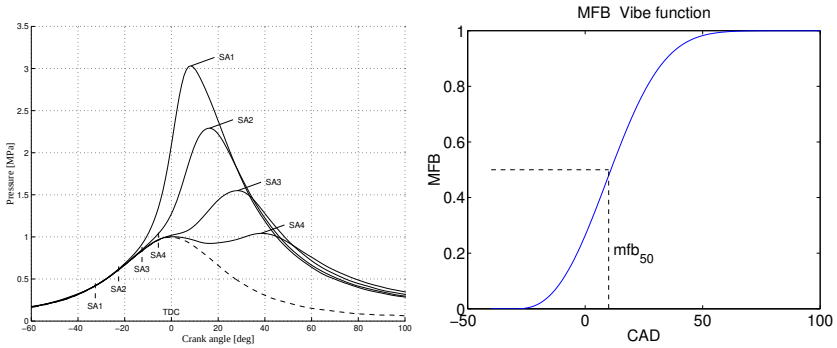

Figure 5.3: *Left: Cylinder pressure from four cycles with different ignition timing. Late combustion gives a higher expansion pressure asymptote. Right: Definition of mfb_{50}. Heat release according to a Vibe function.*

- The cycle with the best combustion phasing has best efficiency and lowest exhaust temperature.
- The best phased real cycles have their 50% mass fraction burned position around 8° ATDC. However, the experiments showed that $MFB_{50,OPT} = 0^o$ ATDC was a better selection.
- The Otto cycle has the best efficiency and lowest exhaust temperature if the combustion is at TDC.

These statements couple the mass fraction burned trace to θ_c in the ideal Otto cycle that defines the volumes at states 2 and 3 to $V_2 = V_3 = V(\theta_c)$.

5.1.3 Combustion part

The pressure ratio management has been investigated in great detail by Matekunas (Matekunas, 1986, 1984, 1983). The pressure ratio is defined using the ratio between the pressure from a firing cycle, $p(\theta)$, and the pressure from a motored cycle, $p_c(\theta)$,

$$\overline{PR}(\theta) = \frac{p(\theta)}{p_c(\theta)} - 1 \tag{5.8}$$

Traces produced by the pressure ratio are similar to the mass fraction burned profiles, for example the position for $\frac{PR(\theta)}{\max(PR(\theta))} = 0.5$ differs only around $1-2°$ from the position for 50% mass fraction burned (Eriksson, 1998). This implies that similar techniques for representing the mass fraction burned profile can be used to simulate the pressure, and this is the method that we have used.

	definition
$\Delta\theta_d$	0-10% burned mass fraction
$\Delta\theta_b$	10-85% burned mass fraction

Table 5.1: *Definition of burn angles.*

Interpolation method

The combustion part is produced by interpolating between the two assymptotic pressure traces p_c and p_e. The interpolation function is the well known Vibe function (Vibe, 1970)

$$PR(\theta) = 1 - e^{-a\left(\frac{\theta-\theta_{SOC}}{\Delta\theta}\right)^{m+1}} \tag{5.9}$$

which gives the following expression for the pressure

$$p(\theta) = (1 - PR(\theta)) \cdot p_c(\theta) + PR(\theta) \cdot p_e(\theta)$$

From the end of combustion to EVO the pressure follows the expansion asymptote, Equation (5.4).

The burn duration $\Delta\theta$ and shape factors a and m in the Vibe function depend on engine speed, air-fuel ratio and EGR ratio. The work presented in (Csallner, 1980; Hires et al., 1978) develop models that addresses these issues. Here these variations are not considered, instead the parameters are specified in terms of the burn angles $\Delta\theta_d$, $\Delta\theta_b$. The burn angles are defined in Table 5.1. Given the burn angles the shape parameters a and m can be calculated the approach here is the same as the one used by Eriksson (1999)

$$m = \frac{\ln\left(\frac{ln(1-0.1)}{ln(1-0.85)}\right)}{\ln(\Delta\theta_d) - \ln(\Delta\theta_d + \Delta\theta_b)} - 1 \tag{5.10}$$

$$a = -\ln(1 - 0.1)\left(\frac{\Delta\theta}{\Delta\theta_d}\right)^{m+1} \tag{5.11}$$

Burn duration can be calculated using flame development angle, $\Delta\theta_d$, and fast burn angle, $\Delta\theta_b$.

$$\Delta\theta \approx 2\Delta\theta_d + \Delta\theta_b \tag{5.12}$$

5.1.4 The remaining parts of the cycle

After the exhaust valve has opened the blow-down phase begins and the pressure approaches the pressure in the exhaust system. For this phase an interpolation scheme can also be used. The same goes for the phase after the intake valve has opened and the cylinder pressure approaches the intake manifold pressure. For the transitions between these two phases a cosine function can be used for the interpolation. These phases are not validated.

5.1.5 Model parameters and inputs

The model is described by a set of inputs and a set of parameters that have physical interpretation. These inputs and parameters are summarized in this section. The tuning parameters are

c_v	specific heat at the combustion
k_c	polytropic coefficient for the compression pressure
k_e	polytropic coefficient for the expansion pressure
q_{HV}	heating value for the fuel
$(A/F)_s$	stoichometric air-fuel mass ratio
T_r	residual gas temperature
x_r	residual gas fraction
θ_{ivc}	intake valve closing angle
θ_{evo}	exhaust valve closing angle
$MFB_{50,OPT}$	optimum position of 50% burned mass fraction

The inputs are

p_{im}	intake manifold pressure
T_{im}	intake manifold temperature
$\Delta\theta_d$	flame development angle
$\Delta\theta_b$	fast burn angle
θ_{SOC}	start of combustion angle
λ	normalized air to fuel ratio

T_r and the residual gas fraction x_r are used as tuning parameter here but they can also be modeled, for example based on cycle simulations. They are important for the model since they directly influence the initial temperature T_{ivc}, Equation (5.3), and the expansion pressure through Equations (5.2) and (5.7). *An illustrative example*: $x_r = 0.07$, $T_{im} = 298$ [K], $T_r = 1000$ [K] yield an initial temperature of $T_{ivc} = 347$ [K], which is a 16% increase. This effect is directly visible in the expansion pressure asymptote.

5.2 Model evaluation

The model consists of a set of parts of which the following will be validated

1. selection of compression pressure
2. selection of compression and expansion polytropic coefficient
3. selection of expansion pressure
4. interpolation between firing and expansion

Finally the influence from air-fuel ratio and ignition timing is studied.

Validation is done in two steps. A model calibration is found to fit the data set best possible. First a general performance is investigated for all data and second a sensitivity analysis is performed on changes in ignition timing, air-fuel ratio and manifold pressure respectively.

5.2.1 Data collection

Two different engines were used for data collection. Engine A is a Daimler Chrysler 3.2L 6 cylinder SI engine and engine B is a Saab 2.3L 4 cylinder SI engine.

The data set for Engine A is a speed-load map of original calibration of ignition and fuel. Engine speed range from 1000 to 5000 rpm and the inlet manifold pressure range from 20 to 100 kPa. The data set from Engine B is taken at 2000 rpm, 100 Nm and with shifted ignition timing and air-fuel ratio.

5.2.2 Compression pressure

The intake manifold pressure gives a good indication of the starting pressure, p_{ivc}, but due to wave effects the initial pressure in the combustion chamber may differ from what is inferred from the intake manifold pressure. There is a possibility to map the initial cylinder pressure as a function of engine speed and load to capture such deviations. Another possibility is to use the air mass flow and volumetric efficiency to support the estimate given by the intake manifold.

Engine A is equipped with an intake manifold pressure sensor positioned close to the intake valve of the cylinder where the cylinder pressure sensor is located. This setup is used to validate how well the intake manifold pressure describes the combustion pressure. The relative error

$$\frac{p_{meas} - p_c}{p_c}$$

at the end of compression was calculated for 89 engine operating conditions. The relative error for all cycles is less than 12%. Adding an affine correction factor for the speed the error was reduced to the range -7–10%, see Figure 5.4. The compression traces are plotted for a big crank interval to show that there is no systematic deviation during the compression. This indicates that the model assumptions for compression holds and deviations comes from in-accuracy in initial data. The variation -7-10% is not large compared to the general variations in the actual cylinder pressure.

5.2.3 Polytropic exponent for compression and expansion

The data set from Engine B was used for polytropic exponent evaluation. For the compression the polytropic exponent was selected to be $k_c = 1.25$. The expansion phase showed a need for a slightly higher exponent, $k_e = 1.30$ was used. Figure 5.5 views the choice of polytropic coefficients for one cycle at

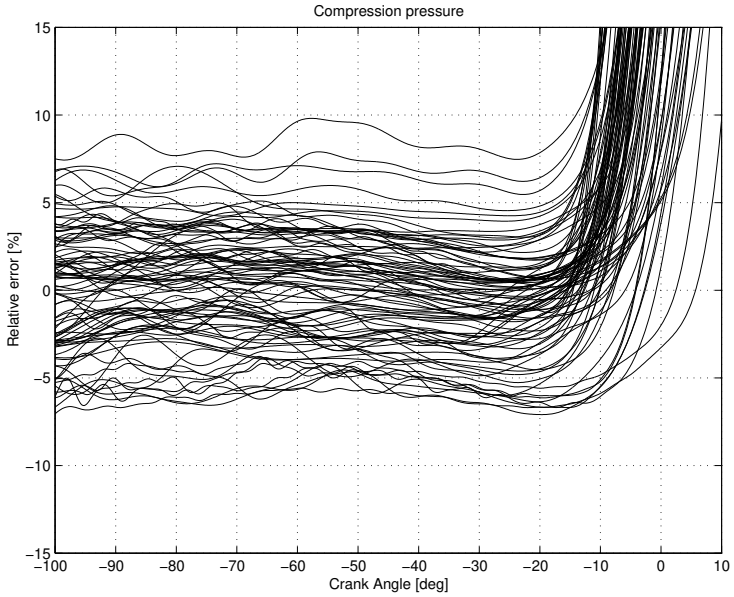

Figure 5.4: *Relative error for compression part, cycle by cycle.*

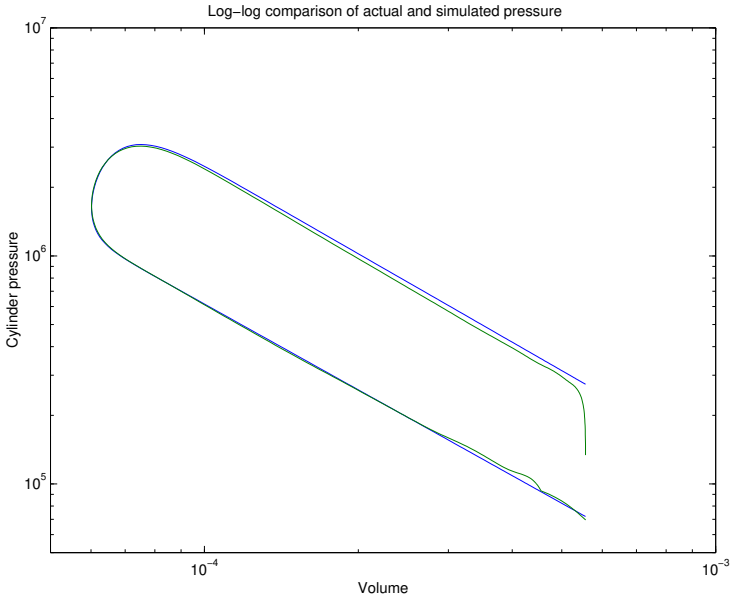

Figure 5.5: *Validation of polytropic coefficient,* $k_c = 1.25$ *and* $k_e = 1.30$

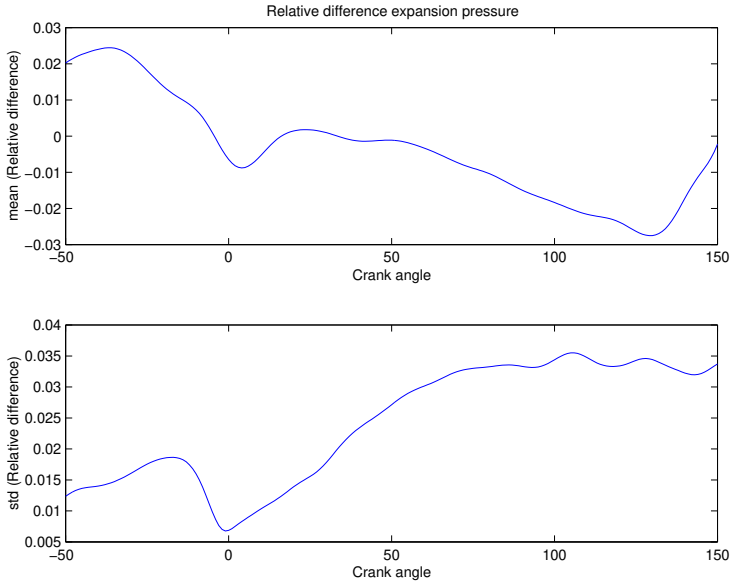

Figure 5.6: *Upper: mean relative error in expansion pressure. Lower: standard deviation in relative error. 2000 rpm, 100 Nm.*

MBT timing and $\lambda = 1$. The important property of the plot is the slope of the compression and expansion parts. Ideally, both the actual and the simulated pressure traces shall have the same slope in the straight parts. In the log-log scale, the slope is the polytropic coefficient. The polytropic coefficient for the compression part is excellent and for the expansion part it is slightly too small. However, in the simulations it was seen that the expansion coefficient has a dependency to engine operating conditions and for engine B $k_e = 1.30$ was the best choice of a constant parameter.

The polytropic coefficients can be modeled to be dependant on engine operating point and it also differs between engines.

5.2.4 Expansion pressure

The expansion pressure level is calculated according to Equations 5.3 to 5.7. Using $T_r = 1000$K and $x_r = 0.07$ produces an overall model performance as in Figure 5.6. Figure 5.6 is based on the full data set from engine B. The highest deviation is seen around peak pressure where the mean error is less than 4% and the standard deviation is 1%. In the expansion part the mean relative difference is less than 2% but the cycle variations have increased to 4%.

The model handles a shift in mfb_{50} position according to Figure 5.7. By shifting ignition timing the timing for mfb_{50} was shifted. The upper graph

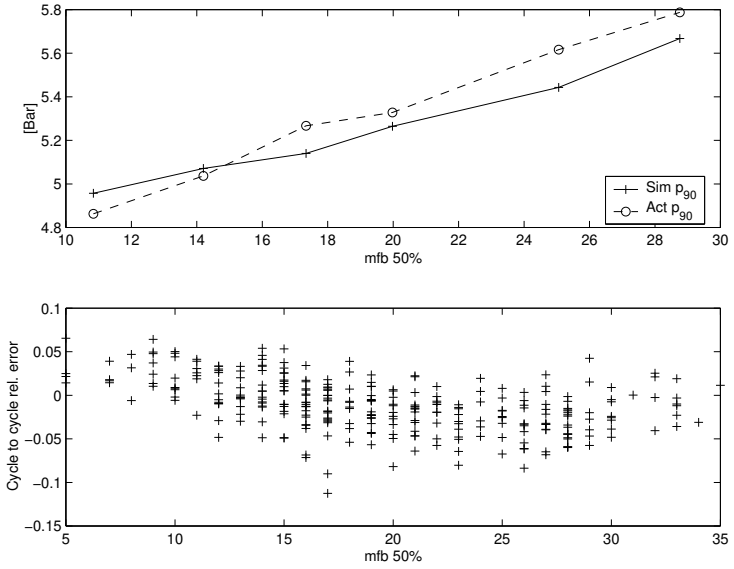

Figure 5.7: *Expansion pressure and combustion timing, modeled and actual. 2000 rpm, 100 Nm.*

shows mean values of the pressure point p_{90}, the cylinder pressure at 90° CAD which is a point where the combustion is finished but before EVO. The main property of the mfb_{50} influence is captured even though there is a difference in slope between operating points. The lower graph shows the relative error between the two p_{90} calculations for each combustion cycle.

5.2.5 Interpolation between compression and expansion

One measure for the model quality of the combustion part is the matching of the peak pressure location (PPL) between simulated and actual pressure. The interpolation is done as in Equation (5.8) with PR defined as in Equation (5.9). The shape factors a and m are calculated from burn angles as in equations (5.10) and (5.11). To validate the pressure model assumptions the burn angles for each cycle were used in the simulation of cylinder pressure. The burn angles were calculated from the pressure trace by first calculating the heat release. The most simple form of heat release analysis was used. It is similar to the method *net heat release* described by Krieger and Borman (1966):

$$dQ = \frac{\gamma}{\gamma - 1} p\, dV + \frac{1}{\gamma - 1} V\, dp$$

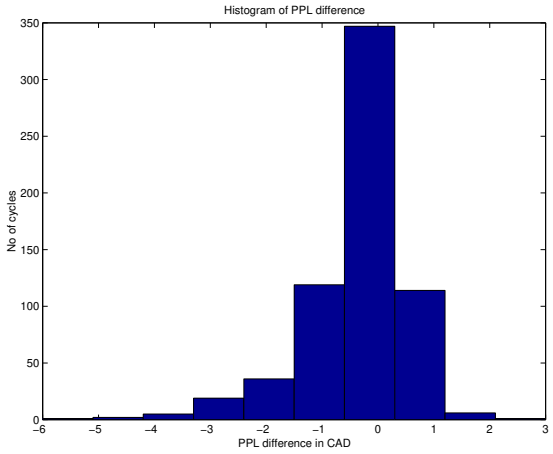

Figure 5.8: *Histogram of difference in PPL, actual and simulated, engine B. This accuracy is attained since the burn angles are considered to be known in this evaluation of the model.*

Mass fraction burned, mfb, is calculated as the integral of heat release

$$mfb(\theta) = \frac{1}{Q_{tot}} \int_{ivc}^{\theta} dQ$$

The burn angles are extracted from the mfb curve according to Table 5.1. Figure 5.8 shows the histogram of the difference in PPL between measured and modeled pressure for each cycle in data set B. The mean value of PPL difference is 0.006 CAD and the standard deviation is 1.1 CAD. The resolution in the sampled pressure data was 1 CAD.

5.2.6 Changes in λ and manifold pressure

Figure 5.9 views the influence from changed air-fuel ratio. In this case there was also a change in mfb_{50} position due to the changed burn speed. The upper graph shows the mean value of relative error. The model captures the behaviour for rich mixtures, where p_{90} decreases when λ decreases from 1. The down slope in the modeled p_{90} for lean mixtures comes from the impact of Equation (5.6) which is obviously not the only effect to consider. Cycle to cycle deviations from the mean error stay at $\pm 7\%$, as seen in the lower graph. Figure 5.10 views the influence on p_{90} when the inlet manifold pressure is changed. Data from engine A is used. The model captures the behaviour of the cylinder pressure at different manifold pressures but a noticeable systematic error is seen. There is a trend where the relative error moves from +20% for low pressure to -30% for high. In the simulations it was noted that the polytropic coefficients k_c

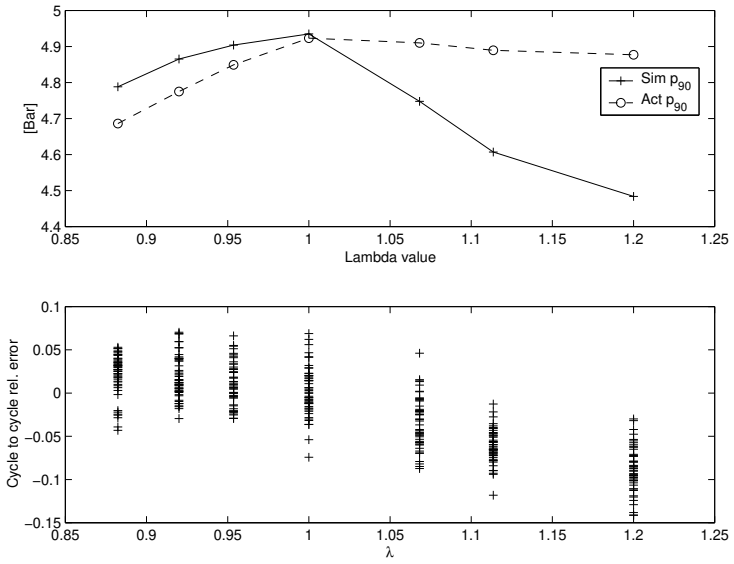

Figure 5.9: *Expansion pressure air-fuel ratio influence, modeled and actual. 2000 rpm, 100 Nm.*

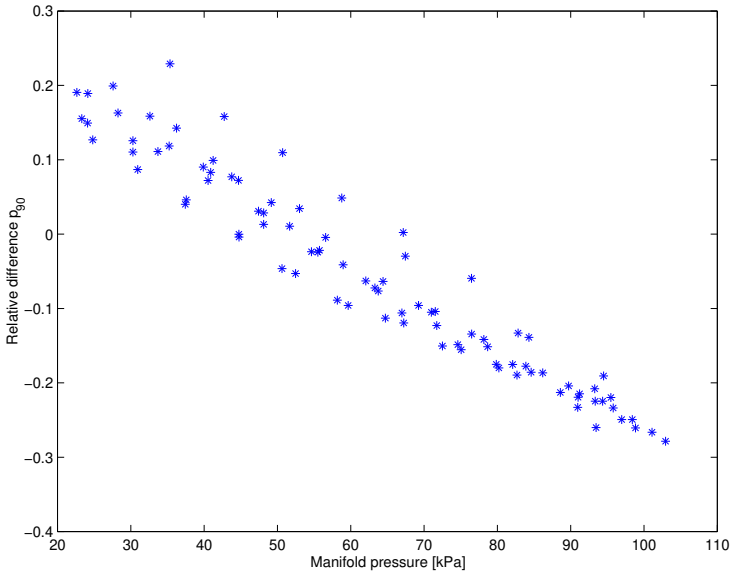

Figure 5.10: *Expansion pressure error, influence from manifold pressure. Engine A.*

and k_e change value significantly. By only changing k_c and k_e it was possible to position the slope in Figure 5.10 at any level and have the error equal to zero for any manifold pressure. This implies a possible enhanced model performance by modeling the polytropic coefficients as a function of engine operating condition.

5.3 Summary and Conclusions

An analytic model for the pressure has been developed and evaluated. The pressure model is given in closed form and there is no need to numerically solve the ordinary differential equations. The model is based on physical relations with components that are easy to measure and tune. The closed expression is

$$p(\theta) = \begin{cases} p_c(\theta) & \theta_{ivc} < \theta < \theta_{soc} \\ (1 - PR(\theta))p_c(\theta) + PR(\theta)p_e(\theta) & \theta_{soc} < \theta < \theta_{evo} \end{cases}$$

and the details in the model are summarized here:

$$\begin{aligned} p_c(\theta) &= p_{ivc}\left(\frac{V_{ivc}}{V(\theta)}\right)^{k_c} \\ T_c(\theta) &= T_{ivc}\left(\frac{V_{ivc}}{V(\theta)}\right)^{k_c-1} \\ p_e(\theta) &= p_3\left(\frac{V(\theta_c)}{V(\theta)}\right)^{k_e} \\ PR(\theta) &= 1 - e^{-a\left(\frac{\theta-\theta_{SOC}}{\Delta\theta}\right)^{m+1}} \\ p_3 &= p_2\,\frac{T_3}{T_2} \\ T_3 &= T_2 + \Delta T_{comb} \\ \Delta T_{comb} &= \frac{(1-x_r)\,q_{HV}\,\eta_f(\lambda)}{(\lambda(A/F)_s + 1)\,c_v} \\ \eta_f(\lambda) &= 0.95\,min(1;\,1.2\lambda - 0.2) \\ p_2 &= p_c(\theta_c) \\ T_2 &= T_c(\theta_c) \\ \theta_c &= mfb_{50} - MFB_{50,OPT} \\ mfb_{50} &= \Delta\theta_d + \frac{1}{2}\Delta\theta_b \end{aligned}$$

$$
\begin{aligned}
T_{ivc} &= T_{af}\,(1 - x_r) + x_r\,T_r \\
V_{ivc} &= V(\theta_{ivc}) \\
p_{ivc} &= p_{im}(\theta_{ivc}) \\
\Delta\theta &= 2\Delta\theta_d + \Delta\theta_b \\
\theta_{soc} &= \theta_{ign} \\
m &= \frac{\ln\left(\frac{ln(1-0.1)}{ln(1-0.85)}\right)}{\ln(\Delta\theta_d) - \ln(\Delta\theta_d + \Delta\theta_b)} - 1 \\
a &= -\ln(1 - 0.1)\left(\frac{\Delta\theta}{\Delta\theta_d}\right)^{m+1} \\
T_{af} &= T_{im}
\end{aligned}
$$

The model contains a number of tuning parameters that effect the accuracy of the pressure model. The tuning parameters are

c_v	specific heat at the combustion
k_c	polytropic coefficient for the compression pressure
k_e	polytropic coefficient for the expansion pressure
q_{HV}	heating value for the fuel
$(A/F)_s$	stoichiometric air-fuel mass ratio
T_r	residual gas temperature
x_r	residual gas fraction
θ_{ivc}	intake valve closing angle
θ_{evo}	exhaust valve closing angle
$MFB_{50,OPT}$	optimum position of 50% burned mass fraction

The inputs are

p_{im}	intake manifold pressure
T_{im}	intake manifold temperature
$\Delta\theta_d$	flame development angle
$\Delta\theta_b$	fast burn angle
θ_{ign}	ignition angle
λ	normalized air to fuel ratio

With a proper tuning of these parameters it is shown that:

- Compression and expansion slopes can be captured well with an accuracy of -7 - 10%.
- When the burn angles are available for the model the peak pressure location stayed within $\pm 1^\circ$ standard deviation from the actual peak pressure location.
- The model can capture large variations in ignition timing.

- The model can capture variations in air to fuel ratio in the rich region.
- Variations in manifold pressure are captured but a significant error trend is seen.

6

A parameterized ionization current model

The parameterized pressure model, described in Chapter 5 gives together with a temperature model an opportunity to study combustion properties by analyzing the ionization current. The focus here is set on the second or the thermal peak of the ionization current. A model is defined with a number of free parameters, which can be estimated by fitting the model to a selected part of a measured ionization current. The model has many parameters where all of them have a physical interpretation. Here, two parameters are chosen to be free, to allow the model to fit to the measured current. The rest of the model parameters are fixed to their best physical value. The two free parameters control position and amplitude of the ionization current.

6.1 Model description

6.1.1 Data collection

A 2.0 liter turbo charged gasoline engine was used for data collection. Data was collected at 2000 rpm with a scan in air-fuel ratio and ignition timing according to Table 6.1. At each operating point (OP) 50 cycles of ionization current and cylinder pressure were recorded. MBTT is the ignition timing for maximum brake torque. This data set was also used for the pressure model validation in Chapter 5.

Engine speed	Ignition angle	Relative air-fuel ratio	OP number
2000	MBTT - (MBTT-15)	1	1-6
2000	MBTT	0.88 - 1.2	7-13

Table 6.1: *Data definition*

Signal	sampling
cylinder pressure	1 CA
ionization current	1 CA
inlet manifold pressure	mean value of 6 samples/cycle
engine speed	once per OP
ignition timing	once per OP
inlet manifold temperature	once per OP
intake air flow	once per OP
air-fuel ratio	once per OP
output brake torque	once per OP

Table 6.2: *Measured signals*

6.1.2 Model definition

The pressure model in Chapter 5 was used with a small change to reduce the number of parameters; the two input parameters in Equations (5.10) to (5.12), flame development angle and fast burn angle, were replaced by one total burn angle and fixed shape factors a and m. The Vibe function in equation (5.9) is

a	20
m	4
$\Delta\theta$	burn angle from ignition, 0-99% burned mass fraction

Table 6.3: *Modification of pressure model*

then calculated without the steps via equations (5.10) to (5.12).

The shape factors a and m were chosen to a mean value of the estimated values from each cycle in the data set. The estimated values of a and m for each cycle were calculated by fitting a Vibe function to the heat release trace. The values are listed in Table 6.3. The burn angle is left as a free parameter for estimation. The burn angle affects both position and amplitude of the simulated ionization current. A longer burn duration delays the peak pressure location and thereby the peak temperature position since the kernel model was used. The slower heat release that results from a longer burn duration decreases the peak pressure amplitude and therefore the peak temperature amplitude.

A kernel zone combustion model, described in Section 4.2, was chosen for

temperature calculation since the position properties showed to be best among the investigated temperature models. To handle the amplitude performance, the initial kernel temperature T_{k0} is left as a free parameter. An increased initial kernel temperature will increase the kernel temperature during the whole combustion and thereby affect the amplitude of the ionization current. Phasing of the current is not affected by the initial kernel temperature, unless the temperature becomes so low that the NO reactions do not reach equilibrium. In that case a lowered initial kernel temperature will also produce a delay of the ionization current peak due to that the NO concentration is still increasing during and shortly after the temperature peak. This effect is relatively small, less than 1° CAD in simulations. In conclusion, the initial kernel temperature can be adjusted to fit the model output in amplitude without changing the position of the same.

NO formation is calculated as a rate controlled process, as described in Section 3.1. The parameters in this part are the reaction constants. The values used are the same as in Section 3.1.

The ionization current calculation is based on the temperature and NO traces. The thermal ionization model contains a number of parameters where most of them are physical constants, see section 3.2. Some parameters describe the geometry of the electric field in the spark gap and other properties of the measurement circuit. These parameters are listed in Table 4.2.

The model equations

The model equations are summarized here. The thermal ionization model is taken from Section 2.2.1 which models the measured current I:

$$I = U\frac{\pi r^2}{d}\frac{e^2}{\sigma m_e\sqrt{\frac{8kT_k}{\pi m_e}}}\sqrt{\phi_s}\sqrt{\frac{2\left(\frac{2\pi m_e kT_k}{h^2}\right)^{\frac{3}{2}}\frac{B_1}{B_0}\exp\left[-\frac{E_1}{kT_k}\right]}{n_{tot}}} \quad [A]$$

$$\phi_s = \frac{[NO]\cdot 10^6}{n_{tot}/N_A} \quad [1]$$

$$n_{tot} = \frac{p}{\tilde{R}T_k}N_A \quad [\text{particles}/m^3]$$

n_{tot} is the particle density in the burned zone, which is located around the spark plug at the time for ionization current measurement, and N_A is Avogadro's constant. The NO formation model is described in Section 3.1:

$$\frac{d[NO]}{dt} = \frac{2R_1(1-([NO]/[NO]_e)^2)}{1+([NO]/[NO]_e)R_1/(R_2+R_3)} - [NO]\frac{1}{V_b}\frac{dV_b}{dt} \quad [mol/(cm^3\cdot s)]$$

The kernel combustion model from Section 4.2 gives the temperature:

$$T_k(\theta) = T_{k0}\left(\frac{p(\theta)}{p_0}\right)^{\frac{\gamma-1}{\gamma}} \quad [K]$$
$$p_0 = p(\theta_{soc}) \quad [Pa]$$

The pressure model $p(\theta)$ is described in Section 5.3 with the change according to Table 6.3.

Initial kernel temperature and flame temperature

The model contains the initial kernel temperature, T_{k0}, as a free parameter. In the kernel zone combustion model in Section 4.2 T_{k0} corresponds to the adiabatic flame temperature. In this model setup T_{k0} is allowed to take lower values than the adiabatic flame temperature to adjust for amplitude. The lower initial kernel temperature still has physical meaning. Since the kernel zone combustion model has no heat transfer part, a reduced T_{k0} adjusts for heat loss to cylinder walls during the combustion. Also, the presence of residual gas reduces the adiabatic flame temperature. The initial kernel temperature can therefore be seen as the flame temperature compensated for residual gas and heat transfer and conclusions about the flame temperature can be drawn from the initial kernel temperature behavior.

6.1.3 Ionization current part selection

The model describes the thermal part of the ionization current. In the optimization process the model output is compared to the measured data, which has to be selected so it represents the model. In the case of this data set, a simple window referenced to the ignition timing was applied to cut out the thermal part of the ionization current, see Figure 6.1. The window is described in Table 6.4. This windowing procedure works for most of the data in the set, but there

Start of window	IGN + 37 CAD
Width of window	50 CAD

Table 6.4: *Cut-out window for ionization current reference*

are cycles where one of the following two phenomena happens:

- a piece of the flame front part entered the window
- the thermal peak falls outside the window

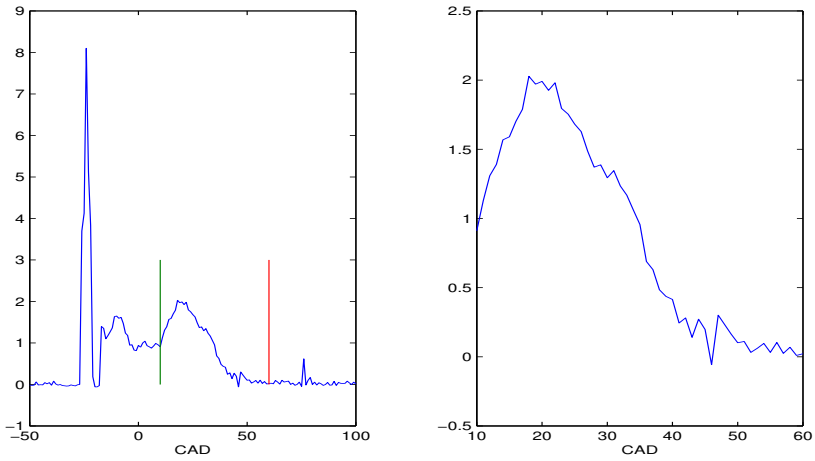

Figure 6.1: *Ionization current window for parameter estimation. Left: the window angles marked with vertical lines, right: the cut-out current*

This was especially seen for operating point 13, at the most lean operation. In both these cases the parameter estimation procedure is successful mathematically, in the sense that it minimizes the error to the chosen reference data. But since the reference data does not correspond to the process we want to model, the free parameters take values that are not realistic in the physical meaning of the model. In other words, the parameter estimation fails.

6.2 Parameter estimation

The model contains two free parameters, burn angle and flame temperature. An optimization function *lsoptim.m* using the Levenberg-Marquardt method finds the optimal values for the two parameters. The function minimizes the sum of squared errors, a penalty function V defined as

$$V(\phi) = \sum_{win}(y - \hat{y}(\phi))^2 \tag{6.1}$$

where ϕ is an array of the free parameters, y is the measured ionization current, $\hat{y}$ is the calculated current and *win* is the defined crank angle window, described in Table 6.4, where the optimization is performed.

Initial guess

The optimization procedure starts at an initial guess of the two free parameters. The initial guess of kernel temperature, T_{k0}, and burn angle, $\Delta\theta_0$, were chosen constant as in Table 6.5.

T_{k0}	1800 K
$\Delta\theta_0$	80 CAD

Table 6.5: *Initial guess of free parameters*

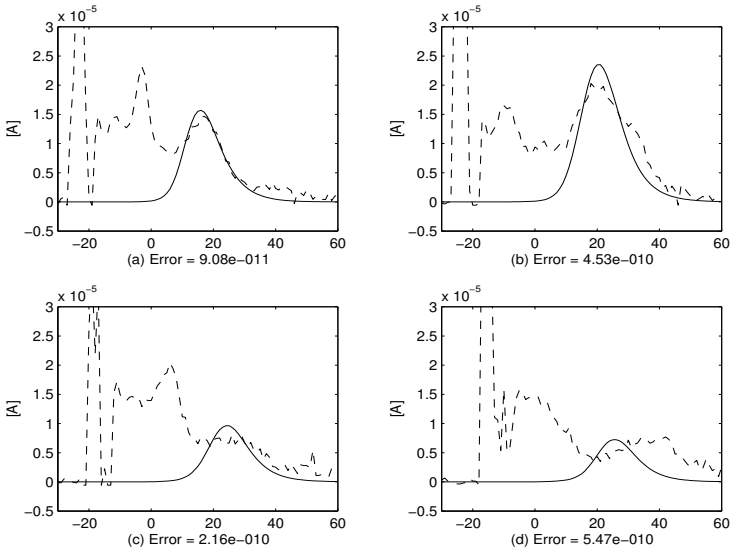

Figure 6.2: *Four randomly picked cycles. Measured and simulated ionization current and the square error of each curve fit. Dotted: measured current, solid: optimized model.*

Results

Figure 6.2 shows four cycles picked from the data set with a measured ionization current and an optimized model. For each cycle the sum of square error is written to relate a value of error to how well a curve fit is done. The left two curve fits shows a sum of square errors of 2×10^{-10}. These two curve fits captures the intended part of the ionization current. The two right curve fits show higher error, around 5×10^{-10}. The upper right shows a good curve fit but the lower right is worse, where the fitted curve should have been positioned futher to the right. In this last case the cut-out did not capture the interesting part of the measured ionization current and therefore the optimization failed. This shows the importance of selecting the cut-out reference data correctly.

The optimization was done for each cycle in the whole data set. Figure 6.3 shows the statistics for the whole data set. Histogram (a) views the distribution of error values. 85% of the cycles have an error of less than $5 \cdot 10^{-10}$. This indicates that most of the cycles are optimized successfully and the windowing

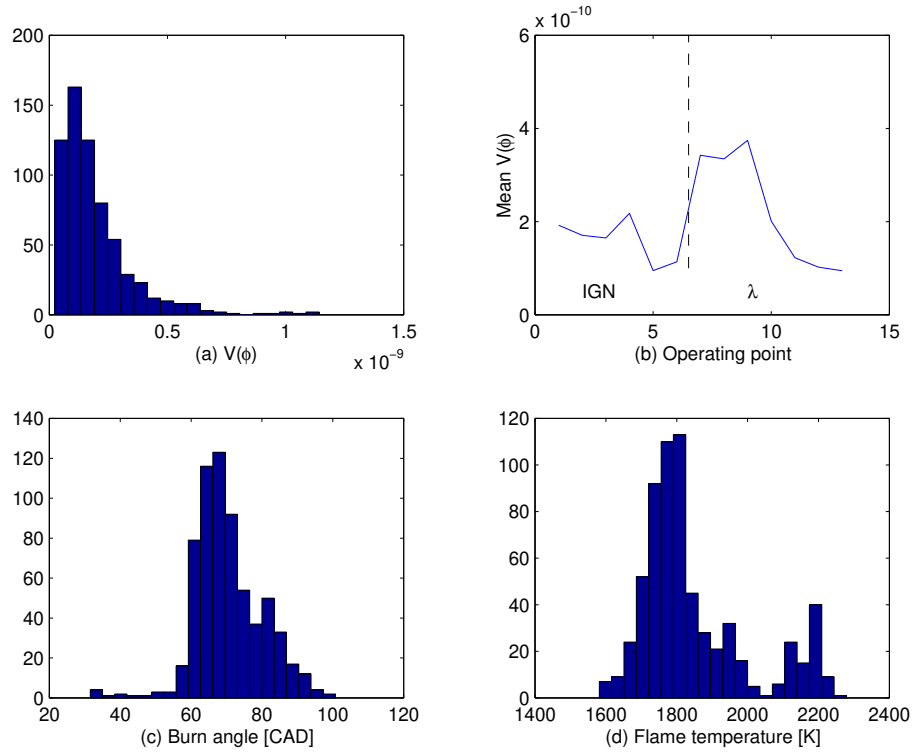

Figure 6.3: *Histogram for (a) $V(\phi)$, (c) burn angle and (d) initial kernel temperature, based on the full data set. (b) shows the mean value of $V(\phi)$ for each operating point in the data set.*

method works well for this data set. The cycles with errors of more than $10 \cdot 10^{-10}$ failed in the optimization and the estimated parameters do probably not reflect the reality. Using the error from the optimization procedure, a tool for accepting or discarding single cycle results is available. To be a more specific selection tool the sum of squared errors needs to be normalized in some sense with the amplitude of the ionization current.

Histogram (c) and (d) shows the distribution in burn angle and flame temperature estimates. Burn angles range from 30 to 100 CAD with the majority of cycles concentrated between 60 and 80 CAD. Flame temperature range from 1600 to 2300K. Comparing to Figure 4.2 where the adiabatic flame temperature is plotted, these estimated temperatures appear reasonable. Residual gas is present in the recorded data set which will dilute the gas mixture and lower the flame temperature. Also, heat transfer will reduce the peak temperature in combustion which in the model will be translated to a lowered initial kernel temperature. Plot (b) of Figure 6.3 shows how the mean value of the penalty function $V(\phi)$ is spread over the 13 operating points. As listed in Table 6.1 points 1 to 6 were recorded at shifting ignition timing and points 7 to 13 at shifting air-fuel ratio.

6.3 Model validation

Figure 6.4 shows the mean values of the parameter estimates for different sets of air-fuel ratio and ignition timing. Plot (a) views the initial kernel temperature estimate at fixed ignition timing and varying air-fuel ratio, and the highest temperature is reached for rich mixtures. When leaning out the mixture the initial kernel temperature falls, which corresponds well with known theory (Heywood, 1988). The burn angle estimate in (b) shows the same linearity as the initial kernel temperature except for the most lean condition. The burn angle is shortest for the richest mixture and longest for the lean mixture. This is also according to known theory (Heywood, 1988). Plots (c) and (d) show the behavior for fixed air-fuel ratio, stoichiometric, and with a varying ignition timing. The phasing of the combustion moves from MBT to later. The initial kernel temperature shows an extremely linear behavior with the lowest value for early ignition and highest for late ignition. One effect hidden here is that the later phasing of the ignition leads to a raised temperature just before combustion starts. The higher gas temperature of the unburned mixture leads to a higher flame temperature. The burn angle also shows a trend where the shortest burn duration appears for MBT timing and the longest for the most retarded ignition timing.

One point fall outside the trend, at ignition timing 18° BTC, as seen in Figure 6.4(d). In this point, OP 4, the loss function V is also higher, see Figure 6.3(b), and it is probably due to that the optimization gets stuck in a local minimum. Another point outside the trend is for a relative air-fuel ratio of $\lambda = 1.2$, see Figure 6.4(b). This point, OP 13, has a low value of the loss function V, but still the optimization fails. The low amplitude of the ionization current

reduces the value of V even though the optimization falis. Poor parameter estimates tend to give shorter burn duration and lower flame temperature than the best visible fit. The optimization procedure shows a sensitivity to the initial guess of the free parameters.

6.3.1 Ion sensing as a virtual cylinder pressure sensor

The model generates a pressure trace as a part of the parameter estimation process. This pressure trace can be compared to the measured cylinder pressure to validate the model assumptions. Three measures are calculated;

1. peak pressure location (PPL)
2. peak pressure amplitude (PPA)
3. burn angle

These three measures are not totally covering the model validation but will give a good idea about the model correctness.

Figure 6.5 shows the evaluation of the pressure trace measures based on both measured and simulated cylinder pressure. Plot (a) compares the mean value of peak pressure location (PPL) in each operating point. The agreement between the model and the measured data is good and the maximum difference in PPL position is 3 CAD except for operating point 13 where the difference is larger, 8 CAD. This is an effect of more unreliable parameter optimization caused by a windowing procedure that sometimes fail to extract the thermal part of the ionization current. As before, when the windowing fails, a part of the flame front is present and dominates the reference data in the optimization procedure. The excess weight in the early part of the window leads to a short burn duration and earlier PPL.

Plot (b) shows the peak pressure amplitude performance of the model. The amplitude of the model follows the measured data well. Again, operating point 13 is worse. Plot (c) shows the performance of burn angle estimate. Generally, the burn angle estimate is a little shorter than the measured data, approximately 10%. The difference is even higher for OP 13, for earlier mentioned reasons. Two points, OP 5 and 6, show only a very small deviation. These points were especially recalculated with a new initial guess of the two parameters. The new initial guess was The new initial guess improved the cylinder pressure estimate

T_{k0}	2200 K
$\Delta\theta_0$	85 CAD

Table 6.6: *New initial guess for OP 5-6*

for OP 5 and 6. The sensitivity of the optimization to the initial guess implies that it can be difficult to find the best fit to every cycle.

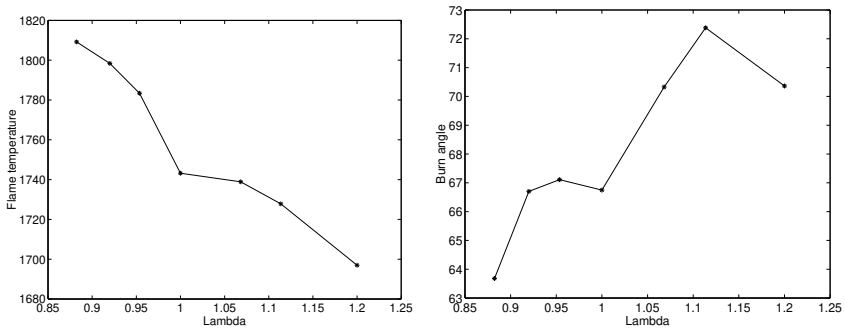

(a) Estimated initial kernel temperature, AFR dependency

(b) Estimated burn angle, AFR dependency

(c) Estimated initial kernel temperature, IGN dependency

(d) Estimated burn angle, IGN dependency

Figure 6.4: *Estimated parameters, initial kernel temperature and burn angle*

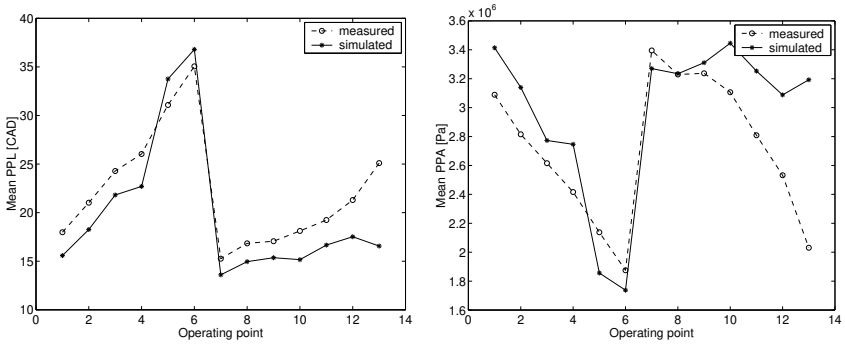

(a) PPL

(b) PPA

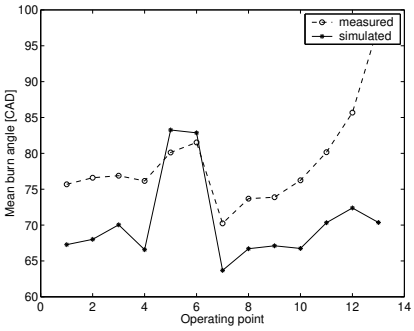

(c) Burn angle

Figure 6.5: *Comparing pressure trace measures from measured and simulated cylinder pressure*

The good agreement between the measured and the simulated pressure data implies that the model assumptions made are relevant. The second peak of the ionization current can be described by a model for thermal ionization. The results also show that the model captures changes in ionization current due to changed ignition timing and air-fuel ratio.

6.4 Conclusions

A model for the thermal part of the ionization current is composed of four modules; an explicit cylinder pressure model, a kernel zone temperature model, a reaction rate controlled NO formation model and a model for thermal ionization.

The model has two free parameters, burn angle and initial kernel temperature. The burn angle affects both position and amplitude of the model output and the initial kernel temperature affects only the amplitude. This model captures the behavior of the ionization current with respect to amplitude and position of the thermal part. The free parameters of the model takes values within physically motivated ranges. Burn angle varies between 30 and 100 degrees with a peak at 60-80 degrees. Estimated initial kernel temperature range is 1600 to 2300 K with a peak at 1800 K. However, it is important to remember that these two parameters have to compensate for effects that are not modeled. One effect is heat transfer, that lowers the peak temperature and therefore lowers the estimated initial kernel temperature in this model.

The model with two free parameters shows good results in calculating the cylinder pressure trace based on optimization to ionization current. The error of the peak pressure location is less than 3 crank angle degrees and the error of the pressure amplitude is less than 20%. This model setup in fact introduces ion sensing as a virtual pressure sensor for spark ignited combustion engines.

7

Conclusions

Ion sensing technology has supported engine management systems for the last 15 years, providing a channel to monitor the combustion process itself. Over the years research started to develop physical models for the ionization process to increase the understanding of the underlying physics. One of the models was designed by Saitzkoff and Reinmann to explain the second peak of ionization currents. This ionization model is combined with cylinder pressure and combustion models and the properties are studied in this thesis.

The thesis includes an investigation of this model in the view of temperature and nitric oxide dependencies. A first conclusion is that a dynamic model for NO formation is as important as the temperature dependent ionization degree for the ionization current amplitude for low temperatures, <2400 K, since NO formation in that lower temperature range is a slow reaction. A second result from this investigation is that the volume change in the burned combustion zone is important to consider when calculating NO formation for a combustion cycle. An extension to the NO formation differential equation presented by Heywood is proposed to handle the influence of combustion development and piston movement on NO concentration.

A model for the second peak of ionization current is presented. The model consists of three parts:

- a combustion temperature model
- a reaction rate controlled NO formation model
- a thermal ionization model

with cylinder pressure as input and ionization current as output of the model.

An investigation of three different combustion models for temperature shows that a kernel zone model best supports the thermal ionization idea. The kernel zone model puts the temperature peak, and therefore also the model output ionization current peak, closest to the measured ionization current peak. Also, the initial kernel temperature can be adjusted to fit the model output in amplitude without changing the position of the same. The main result from this investigation is that thermal ionization can explain the second peak of the ionization current.

Two major contributions of this thesis are the new cylinder pressure model and the parameterized ionization current model that includes the new cylinder pressure model.

The cylinder pressure model expresses the cylinder pressure in closed form as a function of crank angle together with measurable inputs and a set of calibration parameters. The calibration parameters all have a physical interpretation. If the burn angles of the combustion are known, this pressure model captures the cylinder pressure well.

The cylinder pressure model and the second peak ionization current model are put together to form the parameterized ionization current model. The model consists of four parts:

- a cylinder pressure model
- a combustion temperature model
- a reaction rate controlled NO formation model
- a thermal ionization model

The total model has after calibration two free parameters:

- total burn angle
- initial kernel temperature

The total burn angle is a free parameter in the cylinder pressure part and the initial kernel temperature appears in the combustion model. Using this model approach it is possible to estimate burn angle from a measured ionization current. With the estimated burn angle and the pressure model a virtual pressure sensor is available, based on ionization current.

A

Acronyms

ATDC	After TDC
BDC	Bottom Dead Center, engine crank position at ±180 CAD
CAD	Crank Angle Degrees
CHEPP	CHemical Equilibrium Program Package, a MATLAB based software package for calculating chemical equilibrium concentrations in a gas mixture (Eriksson, 2000).
EMS	Engine Management System
EVO	Exhaust Valve Open crank position
IVC	Intake Valve Closing crank position
MBT	Maximum Brake Torque
MBTT	Ignition timing for MBT
SOC	Start Of Combustion crank position
TDC	Top Dead Center, engine crank position at 0 CAD

References

K. Allmendinger, L. Guzzella, and A. Seiler. A method to reduce calculation time for an internal combustion engine model. *SAE Technical Paper no. 2001-mm*, (C448/013), 2001.

I. Andersson and L. Eriksson. Ion sensing for combustion stability control of a spark ignited direct injected engine. *Electronic Engine Controls 2000: Controls*, (SAE Technical Paper 2000-01-0552), 2000.

M. Asano, T. Kuma, M. Kajitani, and M. Tekeuchi. Development of new ion current combustion control system. *SAE paper 980162*, 1998.

J. Auzins, H. Johansson, and J. Nytomt. Ion-gap sense in missfire detection, knock and engine control. *SAE SP-1082*, (SAE paper No. 950004):21–28, 1995.

E. N. Balles, E. A. VanDyne, A. M. Wahl, K. Ratton, and M.-C. Lai. In-cylinder air/fuel ratio approximation using spark gap ionzation sensing. *SAE paper 980166*, 1998.

H. F. Calcote. Ion and electron profiles in flames. *9th Symposium (International) on Combustion*, 1963.

N. Collings, S. Dinsdale, and T. Hands. Plug fouling investigations on a running engine - an application of a novel multi-purpose diagnostic system based on the spark plug. *SAE paper No. 912318*, 1991.

P. Csallner. *Eine Methode zur Vorasberechnun der Änderun des Brennferlaufes von Ottomotoren bei geänderten Betriebsbedingungen*. PhD thesis, Technischen Universität München, 1980.

C. F. Daniels. The comparison of mass fraction burned obtained from the cylinder pressure signal and spark plug ion signal. *SAE Technical Paper 980140*, 1998.

L. Eriksson. Requirements for and a systematic method for identifying heat-release model parameters. *Modeling of SI and Diesel Engines*, SP-1330(SAE Technical Paper no.980626):19–30, 1998.

L. Eriksson. *Spark Advance Modeling and Control*. PhD thesis, Linköping University, May 1999. ISBN 91-7219-479-0, ISSN 0345-7524.

L. Eriksson. Documentation for the chemical equilibrium program package chepp. Technical Report LiTH-R-2298, ISSN 1400-3902, Department of Electrical Engineering, Linköping University, S-581 83 Linköping, Sweden, 2000.

L. Eriksson, L. Nielsen, and J. Nytomt. Ignition control by ionization current interpretation. *SAE SP-1149*, (SAE paper No. 960045):73–79, 1996.

J. Förster, A. Gunther, M. Ketterer, and K-J. Wald. Ion current sensing for spark ignition engines. *SAE 1999-01-0204*, 1999.

D. A. Greenhalgh. Gas phase temperature and concentration diagnostics with lasers. *SAE Technical Paper 834066*, 1983.

M. Hellring, T. Munther, T. Rögnvaldsson, N. Wickström, C. Carlsson, M. L.son, and J. Nytomt. Robust AFR estimation using the ion current and neural networks. *SAE 1999-01-991161*, 1999.

J. B. Heywood. *Internal Combustion Engine Fundamentals*. McGraw-Hill series in mechanical engineering. McGraw-Hill, 1988.

S.D. Hires, R.J. Tabaczunski, and J.M. Novak. The prediction fo ignition delay and combustion intervals for a homogeneous charge, spark ignition engine. *SAE Technical Paper 780232*, 1978.

R.B. Krieger and G.L. Borman. The computation of apparent heat release for internal combustion engines. *ASME paper 66-WA/DGP-4*, 1966.

G.A Lavoie, J.B.Heywood, and J.C.Keck. Experimental and theoretical study of nitric oxide formation in internal combustion engines. *European Journal of Control*, 1, 1970.

A. Lee and J. S. Pyko. Engine misfire detection by ionization current monitoring. *SAE SP-1082*, (SAE paper No. 950003):9–19, 1995.

F. A. Matekunas. Modes and measures of cyclic combustion variability. *SAE Technical Paper 830337*, 1983.

F. A. Matekunas. Spark ignition engines – combustion characteristics, thermodynamics, and the cylinder pressure card. Central States Section, The Combustion Institute, March 19-20 1984. Minneapolis, Mn.

F. A. Matekunas. Engine combustion control with ignition timing by pressure ratio management. US Pat., A, 4622939, Nov. 18 1986.

M. Mladek and L. Guzzella. A model for the estimation of residual gas fraction using cylinder pressure measurements. *SAE Technical Paper 2000-01-0958*, 2000.

L. Nielsen and L. Eriksson. An ion-sense engine-fine-tuner. *IEEE Control Systems (special issue on powertrain control)*, Vol. 18(5):43–52, October 1998.

Y. Nilsson and L. Eriksson. A new formulation of multi-zone combustion engine models. pages 379–387, Karlsruhe, Germany, 2001, 2001. Elsevier Science. 3rd IFAC Workshop "Advances in Automotive Control", Preprints.

R. Reinmann. *Theoretical and Experimental Studies of the Formation of Ionized Gases in Spark Ignited Engines*. PhD thesis, Lund Institute of Technology, April 1998. ISBN 91-628-2985-8, ISSN 1102-8718.

R. Reinmann, A. Saitzkoff, B. Lassesson, and P. Strandh. Fuel and additive influend on the ion current. *SAE Technical Paper 980161*, 1998.

R. Reinmann, A. Saitzkoff, F. Mauss, and M. Glavmo. Local air-fuel ratio measurements using the spark plug as an ionization sensor. *SAE paper No. 970856*, (SAE SP-1263):175–185, 1997.

A. Saitzkoff, R. Reinmann, T. Berglind, and M. Glavmo. An ionization equilibrium analysis of the spark plug as an ionization sensor. *SAE paper No. 960337*, 1996.

A. Saitzkoff, R. Reinmann, and F. Mauss. In cylinder pressure measurements using the spark plug as an ionization sensor. *SAE paper No. 970857*, pages 187–197, 1997.

Y. Shimasaki, M. Kanehiro, S. Baba, S. Maruyama, T. Hisaki, and S. Miyata. Spark plug voltage analysis for monitoring combustion in an internal combustion engine. *SAE paper No. 930461*, 1993.

I.I. Vibe. *Brennverlauf und Kreisprocess von Verbennungsmotoren*. VEB Verlag Technik Berlin, 1970. German translation of the russian original.

H. Wilstermann. *Wechselspannungszündung mit integrierter Ionenstrommessung als Sensor für die Verbrennungs- und Motorregelung*. PhD thesis, University Fridericiana of Karlsruhe, April 1999. ISBN 3-18-338912-6, ISSN 0178-9449.

S. Yoshiyama, E. Tomita, and Y. Hamamoto. Fundamental study on combustion diagnostics using a spark plug as ion probe. *SAE 2000-01-2828*, 2000.

Ya.B. Zeldovich, P.Ya. Sadovnikov, and D.A. Frank-Kamenetskii. Oxidation of nitrogen in combustion. Technical report, Academy of Sciences of USSR, Institute of Chemical Physics Moscow-Leningrad, 1947. Translated by M.Shelef 1970, Ford Motor Company.